Atmos. Chem. Phys. Discuss., 13, 14695–14747, 2013
www.atmos-chem-phys-discuss.net/13/14695/2013/
doi:10.5194/acpd-13-14695-2013

Atmospheric Chemistry and Physics Discussions
Open Access

Climatology of pure Tropospheric profiles and column contents of ozone and carbon monoxide using MOZAIC in the mid-northern latitudes (24° N to 50° N) from 1994 to 2009

R. M. Zbinden[1], V. Thouret[1], P. Ricaud[2], F. Carminati[1,2], J.-P. Cammas[1,3], and P. Nédélec[1]

[1]Laboratoire d'Aérologie, UMR5560, CNRS and Université de Toulouse, Toulouse, France
[2]GAME/CNRM, Météo-France, CNRS URA 1357, Toulouse, France
[3]now at: OSUR, UMS3365, Université de la Réunion, Saint-Denis, La Réunion

Received: 7 May 2013 – Accepted: 14 May 2013 – Published: 5 June 2013

Correspondence to: R. M. Zbinden (regina.zbinden@aero.obs-mip.fr)

Published by Copernicus Publications on behalf of the European Geosciences Union.

Abstract

The objective of this paper is to deliver the most accurate ozone (O_3) and carbon monoxide (CO) climatology for the pure troposphere only, i.e. exclusively from the ground to the dynamical tropopause on an individual profile basis. The results (profiles and columns) are derived solely from the **M**easurements of **OZ**one and water vapour by in-service **AI**rbus air**C**raft programme (MOZAIC) over fifteen years (1994–2009). The study, focused on the northern mid-latitudes [24° N–50° N] and [120° W–140° E], includes more than 40 000 profiles over 11 sites to give a quasi-global zonal picture. Considering all the sites, the pure tropospheric column peak-to-peak seasonal cycle ranges are 23.7–43.2 DU for O_3 and 1.7–6.9 × 10^{18} mol cm^{-2} for CO. The maxima of the seasonal cycles are not in phase, occurring in February–April for CO and May–July for O_3. The phase shift is related to the photochemistry and OH removal efficiencies. The purely tropospheric seasonal profiles are characterized by a typical autumn-winter/spring-summer O_3 dichotomy, (except in Los Angeles, Eastmed – a cluster of Cairo and Tel Aviv – and the regions impacted by the summer monsoon) and a summer-autumn/winter-spring CO dichotomy. We revisit the boundary-layer, mid-tropospheric (MT) and upper-tropospheric (UT) partial columns, using a new monthly-varying MT ceiling. Interestingly, the seasonal cycle maximum of the UT partial columns is shifted from summer to spring for O_3 and to very early spring for CO. Conversely, the MT maximum is shifted from spring to summer and is associated with a summer (winter) MT thickening (thinning). Lastly, the pure tropospheric seasonal cycles derived from our analysis are consistent with the cycles derived from spaceborne measurements, the correlation coefficients being $r = 0.6$–0.9 for O_3, and $r > 0.9$ for CO. The cycles observed from space are nevertheless greater than MOZAIC for O_3 (by 9–18 DU) and smaller for CO (up to 1 × 10^{18} mol cm^{-2}). The larger winter O_3 difference between the two data sets suggests probable stratospheric contamination in satellite data due to the tropopause position. The study underlines the importance of rigorously discriminating between the stratospheric and tropospheric reservoirs and avoiding use of a monthly-

averaged tropopause position without this strict discrimination, in order to assess the pure O_3 and CO tropospheric trends.

1 Introduction

Tropospheric ozone (O_3) is a key parameter for both air quality and climate issues. In the boundary-layer, O_3 is harmful to humans (West et al., 2007), animals and vegetation (Felzer et al., 2007). In the upper-troposphere, O_3 impacts on radiative forcing (Forster and Shine, 1997; Aghedo et al., 2011; Riese et al., 2012). O_3 also controls the oxidizing capacity of the atmosphere. The tropospheric ozone distribution results from complex in-situ photochemical production and interactions with dynamical processes such as stratospheric export (Junge, 1962; Danielsen, 1968; Wernli and Bourqui, 2002; Stohl et al., 2003), free tropospheric subsidence (Guttikunda et al., 2005) or boundary-layer venting (Agusti-Panareda et al., 2005; Auvray et al., 2005) and long-range transport (Cooper et al., 2010). In addition to O_3, carbon monoxide (CO) is also involved in tropospheric photochemical processes: O_3 production takes place when CO and hydrocarbons are photo-oxidized in the presence of nitrogen oxides (NO_x). CO is a by-product of combustion from the boundary-layer and an excellent tropospheric air-mass tracer due to its rather long lifetime of ~ 2 months on average (Yurganov et al., 2004).

Tropospheric O_3 distribution analysis started in the 1960s with soundings that were sparse in space and time (3–12 per month) over about 40 northern hemispheric sites (Logan, 1985, 1994, 1999). Fishman and Larsen (1990) later began tropospheric O_3 retrieval by remote sensing satellites and performed climatology analysis. Nevertheless, satellite observations still cannot replace in-situ measurements because of their need for permanent calibration, their time dependence, low vertical resolution, cloud screening, etc. Since August 1994, the MOZAIC (Measurements of OZone and water vapour by in-service Airbus airCraft; Marenco et al., 1998) instruments onboard commercial aircraft have sampled the troposphere with high vertical resolution over about

Discussion Paper | Discussion Paper | Discussion Paper | Discussion Paper |
ACPD
13, 14695–14747, 2013
Pure Tropospheric O_3 and CO profiles and columns contents
R. M. Zbinden et al.

50 airports and IAGOS (In-service Aircraft for Global Observing System) is the current on-going program (see MOZAIC/IAGOS web site[1]).

The purpose and novelty of the present study are to produce, from the MOZAIC measurements, the first pure tropospheric climatology of O_3 and CO based on fully defined individual tropospheric profiles. The new methodology aims to improve the previous MOZAIC O_3 tropospheric climatology presented by Zbinden et al. (2006) which was restricted by the permanent 12 km limit of MOZAIC aircraft during ascent or descent. Here, all profiles are defined individually from the surface to the dynamical tropopause and include all sampled stratospheric intrusions. Furthermore, the study, based on such new profiles and their associated columns, encompasses a larger range of longitudes from Los Angeles to Japan in the northern mid-latitudes [24° N–50° N].

The paper first briefly describes the MOZAIC data (Sect. 2) and explains the methodology (Sect. 3). The climatological results are presented in Sect. 4 for the monthly-averaged tropospheric columns, the seasonally-averaged tropospheric profiles and the boundary-layer, mid- and upper-tropospheric partial tropospheric columns. To further highlight the usefulness of such a climatology, we compare the O_3 and CO tropospheric seasonal cycles from our analysis with those derived from spaceborne measurements, at two MOZAIC sites in Europe and Asia. Section 5 concludes our analysis.

2 Mozaic data

The MOZAIC programme has collected numerous O_3 observations since 1994 by using instruments onboard five commercial aircraft (Marenco et al., 1998) throughout the troposphere and lower stratosphere. The O_3 is measured using the dual-beam UV absorption principle (Model 49–103 from Thermo Environment Instruments, USA), with an accuracy estimated at ±[2 ppbv + 2 %] and a 4 s time response, i.e. < 50 m vertical resolution (Thouret et al., 1998b). Measurement quality control procedures have re-

[1]http://www.iagos.fr/ or via http://www.pole-ether.fr

ACPD
13, 14695–14747, 2013

mained unchanged to ensure that long-term series are free of instrumental artefacts since the beginning of the programme. Instruments are laboratory calibrated before and after a flight period of about 6–12 months. The infrared CO analyzer (Model 48CTL from Thermo Environmental Instruments, USA) included in the MOZAIC programme since 2001, measured CO with a ±5 ppbv (±5 %) accuracy for a 30 s response time (< 300 m vertical resolution) (Nédélec et al., 2003).

To characterize the vertical distribution over the troposphere, we selected the ascents and descents from the 4 s full-resolution data between August 1994 and March 2009. The results, focused on the northern mid-latitudes [24° N–50° N] and on longitudes from Los Angeles to Japan [119° W–140° E], are based on 11 sites among those most regularly visited by the MOZAIC aircraft (see details in Table 1). To improve the sampling frequency of a few sites and to avoid wide data gaps in the time series, we have created clusters including data from neighbouring airports with the same seasonal cycles and monthly-mean concentrations. For example, Germany is the cluster of Frankfurt and Munich, the most visited site (16 041 profiles). Selecting only Frankfurt would have left data gaps of two months in 2002 and six months in 2005. By adding Munich airport, which is close (500 km) to Frankfurt even though at higher surface altitude (500 m), we obtain continuous time series relevant for climatological studies. Japan is the cluster of Tokyo, Nagoya and Osaka airports on the south-eastern coast (≤ 500 km distance). Houston and Dallas airports form the USsouth cluster (250 km distance). In total, > 40 000 profiles are compiled here (Table 1), i.e. more than twice the number of the profiles used in previous study (Zbinden et al., 2006).

3 Methodology

Our objective is to deliver a monthly-mean pure tropospheric climatology of profiles and columns for O_3 and CO based on the ascent or descent phase of MOZAIC flights, strictly from the surface to the altitude of the dynamical tropopause z_{DT} as defined by Hoskins et al. (1985) (Thouret et al., 2006; Zbinden et al., 2006). However, the troposphere may not be completely sampled by MOZAIC aircraft during individual ascent or descent due to a permanent ≈ 12 km limitation. The tropospheric layer frequently unvisited by MOZAIC was ignored or partially estimated in the previous study by Zbinden et al. (2006). For example, over Germany, the thickness of the tropospheric layer unvisited by MOZAIC is 0.8 km on average but might exceed 3.8 km over Japan in August. In this section, the methodology for deriving the Pure Tropospheric Profiles and Columns is explained, followed by the ozonesonde validation of these new products.

3.1 Pure Tropospheric results assessment

At a specific site, a MOZAIC Profile MP(X,z,t) is defined for a molecule X, such as O_3 and CO at a given time, t, between z_0 and z_{top}, i.e. the surface altitude and the highest altitude of the ascent or descent phase of the flight, with a 50 m resolution in z. The Pure Tropospheric Profile, PTP(X,z,t), should simply result from the MP(X,z,t) without the stratospheric air above z_{DT} at time t. To deliver consistent results between profiles, columns and satellite results, the O_3 volume mixing ratio at a given altitude z and time t is converted into a partial column of 50 m height resolution, expressed in DU (see Zbinden et al., 2006, Appendix A) using its related measured temperature and pressure. Similarly, the CO volume mixing ratio is converted into $mol\,cm^{-2}$. To set up z_{DT} at time t, the potential vorticity pressure of 2-PVU is used. The potential vorticity pressures provided by the operational European Centre for Medium-Range Weather Forecast (ECMWF) analyses (T213) are interpolated for the specific aircraft positions and available with a 150 m vertical resolution on the MOZAIC data base (Thouret et al., 2006; Zbinden et al., 2006).

The methodology to assess the Pure Tropospheric Profiles, explained just below, is illustrated on Fig. 1 with three typical cases selected over Germany ((a) 8 December 1994, (b) 10 May 2000) and Japan ((c) 16 August 1995). Only when $z_{DT} < z_{top}$ (Fig. 1a), the entire troposphere is sampled by MOZAIC. In all other cases, a tropospheric layer remains undefined between z_{top} and z_{DT}, Δ, as shown on Fig. 1b and c. This particular MOZAIC vertical sampling leads to TP(X,z,t), the tropospheric profiles up to z_{DT} or at

ACPD
13, 14695–14747, 2013

least z_{top} at time t, from which a preliminary climatology is calculated on a seasonal basis, $\overline{TP}(X,z,s)$.

In Zbinden et al. (2006), we estimated Δ at time t, using $\overline{TP}(X,z,s)$ above z_{top}. Nevertheless, $\overline{TP}(X,z,s)$ is still strictly limited to z_s, the ascent or descent phase maximum altitude within the season s, and is always less than 12 km. Consequently, Δ is fully evaluated only when $z_{DT} < z_s$, hereafter noted Δ_s (Fig. 1b).

In this study, at time t, if $z_{DT} > z_s$ (Fig. 1c), we additionally evaluated Δ_f between z_s and z_{DT} by using $\mathrm{Mfit}(X,z_{\Delta_f},s)$, the best-fitted line from MOZAIC data using a linear regression on $\overline{TP}(X,z,s)$, from 5 to 11 km for O_3 and from 8 to 11 km for CO.

Our $PTP(X,z,t)$ derivation can be summarized by those three typical cases, where $z = [z_0, z_{DT}]$ at time t:

1. if $z_{DT} < z_{top}$,
   $PTP(X,z,t) = MP(X,z,t) = TP(X,z,t)$;

2. if $z_{top} < z_{DT} < z_s$,
   $PTP(X,z,t) = TP(X,z^\star,t) + \overline{TP}(X,z_{\Delta_s},s)$,
   with $z^\star = [z_0, z_{top}]$ and $z_{\Delta_s} =]z_{top}, z_{DT}]$;

3. if $z_{top} < z_s < z_{DT}$,
   $PTP(X,z,t) = TP(X,z^\star,t) + \overline{TP}(X,z_{\Delta_s},s) + \mathrm{Mfit}(X,z_{\Delta_f},s)$,
   with $z^\star = [z_0, z_{top}]$, $z_{\Delta_s} =]z_{top}, z_s]$ and $z_{\Delta_f} =]z_s, z_{DT}]$.

Figure 2a shows an example of the monthly-averaged MOZAIC O_3 profiles, $\overline{MP}(O_3,z,m)$, and the monthly-averaged pure tropospheric profiles, $\overline{PTP}(O_3,z,m)$, over Japan for September to November and February where the monthly-averaged z_{DT} varies from 9.4 to 13.4 km. This example highlights the profiles $\overline{MP}(O_3,z,m)$ and $\overline{PTP}(O_3,z,m)$ are identical till an altitude, z_{Ld}, where they deeply diverge, located below the monthly-averaged z_{DT}. They show, from the surface to 1 km, a permanent strong

Discussion Paper | Discussion Paper | Discussion Paper | Discussion Paper |
ACPD
13, 14695–14747, 2013
Pure Tropospheric O3 and CO profiles and columns contents
R. M. Zbinden et al.

positive vertical gradient and, above 1 km up to z_{Ld}, a sustainable negative vertical gradient. Above z_{Ld}, $\overline{\mathrm{MP}}(\mathrm{O_3},z,m)$ returns to a positive vertical gradient on the contrary to $\overline{\mathrm{PTP}}(\mathrm{O_3},z,m)$. Thus, z_{Ld}, illustrates the impact of depth penetration of the tropopause and stratospheric air contamination on a monthly basis; this altitude will be used later in Sect. 4.3.1.

Furthermore, the integral along the vertical of $\mathrm{PTP}(X,z,t)$ at time t provides a pure tropospheric column, $\mathrm{PTC}(X,t)$ for a molecule X, such as O_3 and CO, expressed in Dobson Units (DU) and in $\mathrm{mol\,cm^{-2}}$, respectively, with:

$$\mathrm{PTC}(X,t) = \sum_{z=z_0}^{z_{\mathrm{DT}}} \mathrm{PTP}(X,z,t).$$

Moreover, the pure tropospheric columns can be decomposed into three partial columns over the boundary-layer (BLC), mid-troposphere (MTC) and upper-troposphere (UTC). In this study, we have replaced the constant ceiling altitude of MTC (8 km as in Zbinden et al., 2006) by a variable altitude, z_{Ld}, defined as the lowest altitude where $\overline{\mathrm{MP}}(\mathrm{O_3},z,m)$ diverges from $\overline{\mathrm{PTP}}(\mathrm{O_3},z,m)$. An example of the z_{Ld} location over Japan shows variations from 6.0 km in February to 9.0 km in October (Fig. 2a). Thus the partial columns $\mathrm{BLC}(X,t)$, $\mathrm{MTC}(X,t)$ and $\mathrm{UTC}(X,t)$ are integrated over 0–2 km, 2 km–z_{Ld} and $z_{\mathrm{Ld}} - z_{\mathrm{DT}}$, respectively.

The climatologies are given by month (m) for columns (Sect. 4.1), by season (s) for profiles (Sect. 4.2) and by month for the three partial columns considering the new monthly-varying z_{Ld} (Sect. 4.3).

3.2 Pure Tropospheric O_3 validation

This subsection aims to validate the use of $\mathrm{Mfit}(X,z_{\Delta_f},s)$, and finally our $\mathrm{PTP}(\mathrm{O_3},z,t)$ and $\mathrm{PTC}(\mathrm{O_3},t)$, with composite profiles combining $\mathrm{TP}(\mathrm{O_3},z,t)$ from MOZAIC and an external in-situ data set. The latter data came from the World Ozone and Ultraviolet

Radiation Data Center ozonesondes network (WOUDC hereafter) available for neighbouring areas: Wallops Island for USeast, Hohenpeissenberg for Germany and Tateno for Japan.

The WOUDC and MOZAIC data processings are identical. However, to sample similar meteorological situations and improve accuracy, both data sets were selected in time-coincidence (within a 24 h interval, noted t') with a reduced sampling frequency. The time-coincident results by month will be noted m'. Also, we assumed z_{DT} at time t' was valid for both time-coincident data sets. Figure 2b shows the monthly-averaged MOZAIC profiles, $\overline{MP}(O_3, z, m')$, and WOUDC profiles, $\overline{WP}(O_3, z, m')$, over Japan for the four months as provided on Fig. 2a. The best agreement between those monthly-averaged profiles is found when z_{DT} is greater than 12 km on a monthly average. This is an important result because, in such high z_{DT} cases, the troposphere is not fully sampled with MOZAIC. After discarding the stratospheric air above z_{DT} at time t', the monthly-averaged pure tropospheric profiles were derived from MOZAIC and WOUDC as $\overline{MPTP}(O_3, z, m')$ and $\overline{WPTP}(O_3, z, m')$, respectively (Fig. 2c). Despite z_{DT} uncertainties and/or co-location errors at time t', it is interesting to note that, as in Zbinden et al. (2006), both time-coincident tropospheric climatologies exhibit the same almost straight negative O_3 vertical gradient above 3 km (also clearly observed in summer over USeast but not shown).

Then, to validate the estimation of Δ on the full MOZAIC data set, we derived a composite profile called MOZAIC-WOUDC pure tropospheric profiles, $MWPTP(O_3, z, t)$, by adding $\overline{WPTP}(O_3, z_\Delta, m')$ to $TP(O_3, z^\star, t)$ over Δ with $z = [z_0, z_{DT}]$, $z^\star = [z_0, z_{top}]$ and $z_\Delta =]z_{top}, z_{DT}]$. Only two cases needed to be considered:

1. if $z_{DT} < z_{top}$,
   $MWPTP(O_3, z, t) = TP(O_3, z, t) = PTP(O_3, z, t)$;

2. if $z_{top} < z_{DT}$,
   $MWPTP(O_3, z, t) = TP(O_3, z^\star, t) + \overline{WPTP}(O_3, z_\Delta, m')$.

Before providing such a composite result, we checked the consistency of the MOZAIC and WOUDC time-coincident data sets between 2 and 8 km, $\overline{\mathrm{MPTP}}(\mathrm{O_3}, z, m')$ and $\overline{\mathrm{WPTP}}(\mathrm{O_3}, z, m')$. We selected the three most documented and distant sites (USeast, Germany, Japan). The altitude limitation was necessary to avoid the highly variable boundary-layer and to take into account the layers with the best MOZAIC sampling rate below z_{DT}. We found the correlation coefficient is $r > 0.9$ (Fig. 3). Moreover, when integrating the two MOZAIC and WOUDC data sets, the differences were −0.01 DU (−7 %), −0.003 DU (−2 %) and 0.008 DU (0.9 %) on average for USeast, Germany and Japan, respectively. The high and regular sampling frequency over Germany of both data sets as the small z_{DT} variability contributes to the best quality of results. Furthermore, a WOUDC O_3 excess occurred over USeast whatever the month, over Japan during May–September, and over Germany only in March (Table 2). The German range was [0–1 DU] or [0–5 %] and extreme values are −3.1 DU (14 %) in August over USeast and 1.7 DU (9 %) in February over Japan. Therefore, we consider that our Δ estimate can now be validated by comparing the $\overline{\mathrm{PTP}}(\mathrm{O_3}, z, m)$ with the composite result $\overline{\mathrm{MWPTP}}(\mathrm{O_3}, z, m)$.

Finally, using all MOZAIC data sets, we validated the methodology by checking the consistency of $\overline{\mathrm{TC}}(\mathrm{O_3}, m)$, $\overline{\mathrm{PTC}}(\mathrm{O_3}, m)$ and $\overline{\mathrm{MWPTC}}(\mathrm{O_3}, m)$, the vertical integration of $\overline{\mathrm{TP}}(\mathrm{O_3}, z, m)$, $\overline{\mathrm{PTP}}(\mathrm{O_3}, z, m)$ and $\overline{\mathrm{MWPTP}}(\mathrm{O_3}, z, m)$. Figure 4 shows their seasonal cycles for USeast, Germany and Japan with, in addition, their associated z_{DT} and z_{top}. The three sites clearly show the same $\overline{\mathrm{PTC}}(\mathrm{O_3}, m)$ and $\overline{\mathrm{MWPTC}}(\mathrm{O_3}, m)$ seasonal cycles. The bias between $\overline{\mathrm{MWPTC}}(\mathrm{O_3}, m)$ and $\overline{\mathrm{PTC}}(\mathrm{O_3}, m)$ is less than 2 DU or (6 %). Therefore, as $\overline{\mathrm{PTC}}(\mathrm{O_3}, m)$ and $\overline{\mathrm{MWPTC}}(\mathrm{O_3}, m)$ correlation coefficient is $r > 0.96$, we conclude that the method is successfully validated for O_3. The linear $\mathrm{Mfit_s}$, derived from MOZAIC for O_3 between 5 and 11 km, is particularly suitable to fill Δ_f. Consequently, $\mathrm{PTP}(\mathrm{O_3}, z, t)$ and $\mathrm{PTC}(\mathrm{O_3}, t)$ may be derived without the use of data external to the MOZAIC data set.

To summarize, in order to provide the pure tropospheric profiles PTP(O_3, z, t) when $z_{top} < z_s < z_{DT}$, we updated the methodology presented in Zbinden et al. (2006) by adding $Mfit_s$ to TP(O_3, z, t). The methodology was validated over three different sites, each located on a different continent, by using WOUDC time-coincident data sounding. We concluded that the seasonal cycles of the composite MOZAIC-WOUDC tropospheric columns were positively biased, always by less than 2 DU (6 %), compared to the pure tropospheric ozone column. This result allows us to use this methodology on sites not documented by sondes. PTP(O_3, z, t) and PTC(O_3, t) at time t are finally estimated without any data external to the MOZAIC data set, which is a major advantage. Additionally, to obtain purely tropospheric columns for CO, a similar methodology is applied as 90 % of the column amount resides well below 12 km with a maximum weight in the lowermost troposphere. Thereafter, in the text and the figures that follow, we will use $MP_s(X)$, $TP_s(X)$ or $PTP_s(X)$ for averaged-profiles at season s and $TC_m(X)$ or $PTC_m(X)$ for averaged-columns at month m and for a given molecule X, O_3 and CO.

4 Results

In this section, the methodology is applied to the 11 MOZAIC sites to derive three types of climatological products: (1) the monthly-averaged pure tropospheric columns $PTC_m(X)$; (2) the seasonally-averaged pure tropospheric profiles $PTP_s(X)$; (3) the monthly-averaged partial columns: $BLC_m(X)$, $MTC_m(X)$ and $UTC_m(X)$. Finally, $PTC_m(X)$ is compared to satellite results.

4.1 Pure tropospheric column seasonal cycles

The $PTC_m(O_3)$ and PTC_m(CO) cycles are given on Figs. 5 and 6, respectively. On Fig. 5, at all sites, the $TC_m(O_3)$ cycles, the flat z_{top} and the z_{DT} are additionally provided. Over all months in Europe, the value of Δ is < 1.5 km. In contrast, Δ is up to 3 km in summer at the other sites while, in USsouth and Uaemi between 1 and 4 km all over the months due to intense domestic traffic. The numbers of monthly O_3 profiles (1994–2009) and CO profiles (2002–2009) are given on Figs. 5 and 6, respectively. The best sampling rate is obviously over Germany. USeast, Paris, Vienna, and Japan, still regularly visited, are sampled more than twice a week, which corresponds to the best ozonesonde sampling rate. Irregular visits over the 15 yr lead to the lowest MOZAIC sampling frequency over Uaemi, Los Angeles and Eastmed. To further characterize the representativeness of sites, the Figures also include statistics on inter-annual variability: box for the quartiles Q25, Q50, Q75 and whiskers for the inter-quartile range (IQR=Q75-Q25). No box means that only one month has been documented over the period.

4.1.1 Ozone seasonal cycle

Considering all the sites, $PTC_m(O_3)$ varies from a European minimum of 23.7 DU in December to a Middle East maximum of 43.2 DU in July. Below, we detail regional characteristics.

- The *European* $PTC_m(O_3)$ *cycles* exhibit homogeneous patterns with a small summer maximum and a weak amplitude (i.e. from peak-to-peak here and therafter) associated with a positive west-east gradient. Paris and Germany behave similarly and $PTC_m(O_3)$ are within 24.3 DU in winter and 35.6 DU in summer. Vienna differs slightly by reaching a summer maximum of 38.4 DU, probably due to its continental location and polluted air masses coming from the western part of Europe or the Po Basin (Baumann et al., 2001). As the z_{DT} variability is the weakest, the results obviously highlight the impact of photochemistry due to local or remote emissions of O_3 precursors and long-range transport.

- The *Asian* $PTC_m(O_3)$ *cycles*, i.e. Beijing and Japan, vary from 25–26 DU to 40–41 DU, with a strong similarity from December to May. We point out a strong regional contrast in June, when Beijing reaches a maximum and Japan declines sharply due to incoming O_3-poor maritime air during the summer monsoon, con-

ACPD
13, 14695–14747, 2013

sistent with what Logan (1985, 1999) reported from sonde analysis. In addition, z_{DT} over Japan is 2.5–5 km higher than over Beijing from July to September. Interestingly, of all the sites studied, Japan has the lowest amounts of summer O_3 due to the impact of the monsoon. Thus, over Beijing, the higher CO compared to Japan (see Sect. 4.1.2), with probably higher NO_x (Lamsal et al., 2011), are favourable to higher O_3 in July, in spite of the summer monsoon. Note that Wang et al. (2012) reported far greater O_3 tropospheric columns, up to 38 DU in winter and 70 DU in summer, over Beijing using sondes launched at 14:00 LT from 2002 to 2010 and taking the 2 °C km^{-1} lapse rate criterion for the tropopause. Firstly, their yearly-averaged 46 DU, given for a 0–9 km partial column with a 4–5 % yr^{-1} increase, is far greater than our monthly summer maximum. Secondly, their monthly tropopause is located between 9 km (winter) and > 14 km (summer), 2 km above ours. Thirdly, their (MOZAIC) monthly-averaged O_3 volume mixing ratios in summer between 9 km and the tropopause, which are in the 140–600 ppbv range (180 ppbv maximum), suggest a plausible stratospheric air contamination. These combined factors obviously lead to much higher tropospheric columns than the pure tropospheric columns presented in our analysis.

- The *North American* $PTC_m(O_3)$ *cycles* show different patterns from bimodal over the south (Los Angeles and USsouth), slightly bimodal over USlake, to perfectly unimodal over USeast. The z_{DT} variations probably contribute to the northern US cycle differences. The USeast cycle is close to that found in Europe despite a larger peak-to-peak range [24–40 DU (December–June)]. The USlake cycle exhibits two maxima, in May and July (38 DU), with one local minimum in June (37 DU), surprisingly also detected on southern US sites. In the southern US, Los Angeles, rather poorly and irregularly monthly sampled (< 42 monthly profiles; March sampled only in 2005 and November only in 2004), shows two maxima (40 DU in May, 37 DU in July–August). The spring maximum, the biggest over the US, is related to the pollution exported from Asia (Jaffe et al., 2003, 2007; Parrish et al., 2004; Cooper et al., 2006, 2010; Brown-Steiner and Hess, 2011). In sum-

ACPD
13, 14695–14747, 2013

mer, the secondary peak appears rather small, despite a high z_{DT}, due to strong influence of subtropical Pacific air masses (Oltmans et al., 2008). In addition, during wintertime, the O_3 exceeds 27 DU in Los Angeles and is in the range of the Asian sites. The two modes of the USsouth seasonal cycle are inverted compared to Los Angeles with 38.8 DU in April–May and 36.8 DU in July–August. The summer maximum of USsouth, highly enhanced compared to $TC_m(O_3)$ due to high z_{DT}, is now more consistent with the results reported by Cooper et al. (2006) and Li et al. (2005).

- The *Middle Eastern* $PTC_m(O_3)$ *cycles* show a high June–July maximum: 39.7 DU (Uaemi) and 43.2 DU (Eastmed). The Eastmed maximum is even larger than the Beijing maximum. Both appear to be in agreement with the summer extremes shown on the OMI/MLS[2] climatology produced by Ziemke et al. (2011). The Uaemi cycle is the flattest (11.9 DU amplitude) due to an extremely high and steady z_{DT} (> 14 km, except in December) and thus is greater than 33 DU from January to October. In contrast, the Eastmed cycle amplitude is 16.7 DU, the highest among all sites, associated with a 5 km z_{DT} amplitude. Intense photochemical activity is detected there in spring. In May, z_{DT} is 15 km (11 km) over Uaemi (Eastmed) while O_3 amounts are 37 DU (41 DU). Consequently, a high z_{DT} does not necessarily imply a high $PTC(O_3)$. Note that, over Eastmed, the highest variability of all sites (7 DU IQR in May and September) is linked to irregular monthly sampling. Despite sporadic regional sampling, MOZAIC contributes to the tropospheric-chemistry mapping of this area undocumented by ozonesondes.

This quasi-hemispheric overview of the $PTC_m(O_3)$ seasonal cycle shows an overall minimum in Europe, a summer maximum over the northeastern US, a spring-summer maximum that is extreme in the Middle East and strong in Asia. The Asian summer monsoon results in an abrupt decline in June over Japan, unlike over Beijing where pollutants such as CO, and probably NO_x, are exceptionally

[2]Ozone Monitoring Instrument/Microwave Limb Sounder.

ACPD
13, 14695–14747, 2013

high, leading to a sharp geographical contrast in O_3. Furthermore, it is noteworthy that Japan, in summer, exhibits the lowest pure tropospheric O_3 amounts of all the sites studied. The Asian/south-western US connection is predominant in spring and their cycle patterns show some similarity. Over Uaemi, a high and rather steady z_{DT} strongly impacts the O_3 seasonal cycle, as seen in late-winter and early-spring, in contrast with Europe, where photochemistry, local emissions and long-range transport predominate. The European cycle patterns, very similar to those of the northern US, confirm a common source of variance. The low German IQR is related to the higher sampling quality and, probably, low z_{DT} seasonal variability.

4.1.2 Carbon monoxide seasonal cycle

Here, we present another new result derived from MOZAIC. Figure 6 shows $TC_m(CO)$ and $PTC_m(CO)$ for all the sites with a scale change for Beijing to accommodate with its high level of pollution. Since CO measurements have started in January 2002, the monthly sampling frequency is given on the Fig. 6. Germany has the greatest sampling rate with at least 706 profiles/months, followed by Vienna (109–228), Japan (65–128) and USeast (81–154) or USlake (43–162). The poorest statistical significance is in February over Beijing (no box-and-whisker) because this month is documented only in 2003. The Δ filling added to derive $PTC_m(CO)$ is less than 0.1×10^{18} mol cm^{-2} over Europe and is the greatest, $\sim 0.3 \times 10^{18}$ mol cm^{-2} (16 %), over Japan and Uaemi in August. It is interesting to compare Δ with the remote sensing errors. SCIAMACHY[3] error range is 0.05–0.1 × 10^{18} mol cm^{-2}; ACE-FTS[4] has ∼ 16 % bias between 5 and 12 km on 108 MOZAIC coincidences (Clerbaux et al., 2008) and reaches 40 % in UT (Hegglin et al., 2008); MOPITT[5] exhibits a positive bias at all altitudes, stronger at 750 hPa (25 %)

[3] SCanning Imaging Absorption spectroMeter for Atmospheric CHartographY.
[4] Atmospheric Chemistry Experiment Fourier Transform Spectrometer.
[5] Measurements Of Pollution In The Troposphere.

ACPD
13, 14695–14747, 2013

than at 250 hPa (9 %) leading to a mean bias of 19 % on total column (Emmons et al., 2009) with a noticeable instrumental drift (Emmons et al., 2004, 2007). Thus, our Δ added to obtain $PTC_m(CO)$ is less than or equivalent to remote sensing errors (except in cases of intense domestic traffic). At northern mid-latitudes, the $PTC_m(CO)$ range is $1.7–6.9 \times 10^{18}$ mol cm^{-2}. All minima occur during June–November and the maxima occur in early spring except in Vienna, Beijing, Uaemi and Eastmed, all of which occuring earlier, in winter.

– The *North American* $PTC_m(CO)$ *cycles* show an April maximum, except USeast (March), and a September minimum, except USsouth (July). Over all these sites, a sharp May–June CO depletion highlights the intense photochemical activity. The northern US cycles differ by less than 0.1×10^{18} mol cm^{-2} and exhibit patterns more comparable to Europe than to any other sites, due to the CO lifetime and strong connection through westerlywinds. The July bump over USeast results from the impact of North American boreal fires, during the summer of 2004 (Turquety et al., 2007). These two sites show a June–October excess of CO (up to 0.3×10^{18} mol cm^{-2}) compared to the southern US sites. USsouth shows a June–October wide flat minimum, probably related to the pollution lifted under the influence of a semi-permanent anticyclone over Texas and the active summer convection that helps lifting the surface pollution to the mid-troposphere (Li et al., 2005; Liu et al., 2006). The Los Angeles amplitude is 50 % greater than in the other US cycles. The winter-spring maximum is almost equivalent to that of the northern US sites while the September deep narrow low summer minimum seems to be related to the impact of the depleted polluted air from Asia or clean air from southern Pacific, which appears consistent with the O_3 observations.

– The *European* $PTC_m(CO)$ *cycles* vary from 1.9 to 2.7×10^{18} mol cm^{-2}. The IQR over Germany are the steadiest, with less than 0.25×10^{18} mol cm^{-2} and highlight the impact of the sampling frequency as seen by comparing June on the 3 European sites. The sharp depletion in May–June, already seen over the US, is

ACPD
13, 14695–14747, 2013

evidence of the powerful OH cleansing efficiency regulated by NO_x (Lamsal et al., 2011). Later, the seasonal cycle remains almost unchanged from June to November (Paris) or starts a very slow increase in August (other European sites) related probably to remote fires emission. Interestingly, wintertime shows higher amounts over Vienna than over Paris (10 %) or Germany because of its downwind position in Europe or the influence from the Po Valley.

- The *Middle East* PTC_m(CO) *cycles* are both in the same range. They show the lowest PTC_m(CO) in winter and comparable weakest seasonal cycle amplitudes ($1.8–2.3 \times 10^{18}$ mol cm^{-2}), explained probably by the smallest contribution of local CO emissions. Focusing on Dubai, Tangborn et al. (2009) experimented MOZAIC using the assimilated SCIAMACHY CO data. With favourable cloud-free conditions, they had to reduce by 10 % the OH and doubled the CO emissions in the model to lessen the total CO column differences with their MOZAIC independent data set from 1.0 to 0.6×10^{18} mol cm^{-2}. Nevertheless, their MOZAIC data set did not take account the extremely large unvisited tropospheric remainder, we estimated to be ∼ 10 % of PTC_m(CO) on a yearly average performed in 2004 and greater than 0.3×10^{18} mol cm^{-2} in October, i.e. equivalent to the amplitude of the seasonal cycle. Over Eastmed, due to the spring low PTC_m(CO) in May–June, the CO does not appear to be the most important spring source of O_3 here and thus the large amount of $TC_m(O_3)$ appears here as more consistent with intense stratosphere-troposphere exchanges (STE), NO_x contribution or a long-range transport hypothesis. In summer, CO remains in the same range as over Europe, far less than in Asia.

- The *Asian* PTC_m(CO) *cycles* exhibit the highest CO amounts. They are extremely favourable to O_3 production when combined with the highest NO_x amount on the hemisphere scale as detected from satellites over China, during 1996–2005, and related to human activity (van der A et al., 2008; Schneider and van der A, 2012). The Beijing seasonal cycle has a 3.4×10^{18} mol cm^{-2} March minimum, exceeding the Japanese one, and a 6.9×10^{18} mol cm^{-2} winter maximum, more than twice those of all the other sites studied. These highest values are associated with the largest inter-annual variability (see Beijing, in December sampled by 10 profiles) and we noted Beijing in February was only sampled in 2003 (no box and whiskers). The Japanese cycle peaks in March (3.0×10^{18} mol cm^{-2}), reaches a minimum in August (2.3×10^{18} mol cm^{-2}) and has an irregular IQR from 0.1 to 0.4×10^{18} mol cm^{-2}. Finally, whatever the season and prevailing winds considered, the air masses over Beijing are systematically CO enriched by a factor of 1.2–2.8 compared to Japan.

4.2 Pure tropospheric profiles

To complement the tropospheric column climatology, the $PTP_s(O_3)$ and $PTP_s(CO)$ are provided to evaluate the vertical anomalies more precisely from a regional point of view. The North American, European and the Eastern sites are grouped together on Figs. 7, 8 and 9, respectively. The $PTP_s(X)$ are plotted up to the seasonal mean z_{DT}, between 9.5 and 15 km. This complementary information along the vertical allows further analysis shedding light on origin of the two chemical species. For this reason, the O_3 (top row) and CO (bottom rows, i.e. 0–2 km and 2–15 km) are on the same Figure for each region.

4.2.1 North American profiles

The results are plotted on Fig. 7. Over the northern US, the $PTP_s(O_3)$ show the typical autumn/winter and spring/summer seasonal dichotomy as previously described in Zbinden et al. (2006). This is the typical seasonal behaviour of the vertical pure tropospheric ozone distribution in northern mid-latitudes. It characterizes the photochemical activity leading to O_3 production. The $PTP_s(CO)$ presents a different dichotomy in the free troposphere with a winter/spring maximum and a summer/autumn minimum; the minimum being related probably to the higher amounts of OH at that time. Over the

ACPD
13, 14695–14747, 2013

southern US, the seasonal vertical distributions are slightly different. Over USsouth, the summer O_3 profile, between 1 and 4 km, reveals the O_3-poor monsoon flux impact. Among all the sites, we found the lowest amounts of CO here in the summer BL, because the high OH amounts shortened its lifetime. Between 6 and 9 km, quantities of O_3 are enhanced, probably due to additional O_3 from $LiNO_x$ production, especially in summer (Li et al., 2005). This counterbalances the low amounts of O_3 in the BL and explains why the tropospheric columns in summer are still maximized (Fig. 5). In autumn, the amounts of O_3 in the BL are higher than in winter and thus the typical dichotomy is strongly modified. Such characteristics are also observed over Los Angeles and Beijing (see below). Considering now Los Angeles, the typical autumn/winter and spring/summer seasonal dichotomy is not found. The profiles exhibit fine structures along the vertical, probably accentuated by the low MOZAIC monthly sampling rate. However, the spring O_3 spikes of +0.03 DU between 2 and 7 km are indications of long-range transport from Asia (Jaffe et al., 2003; Parrish et al., 2004; Cooper et al., 2005; Neuman et al., 2012). The summer O_3 profile, above 1 km, is unusually close to the autumn-winter one (less than 0.02 DU difference) while the CO is extremely low due to air coming from the southern Pacific (Oltmans et al., 2008; Neuman et al., 2012). In contrast, below 1 km, the highest summer maximum of all the sites studied (0.28 DU) is probably explained by the lack of deep convection (Cooper et al., 2006). The winter CO is higher than elsewhere in the US. Thus, the secondary peak of the $PTC_m(O_3)$ cycle, in summer, depends on a high z_{DT} and on heavy local pollution as O_3 in the BL reaches 0.28 DU (maximum of the all study) with high CO up to 3×10^{16} mol cm^{-2}.

4.2.2 European profiles

The European O_3 profiles (Fig. 8) present similar seasonal dichotomies and are comparable to the two northern US ones (Fig. 7). Nevertheless, we found the following: (1) O_3 excess all throughout the troposphere explains the higher $PTC_m(O_3)$ over Vienna; (2) the greatest spring CO amounts above 2 km over Paris are indications of long-range pollution transport by the westerly wind from the west coast of the US; (3) during win-

ACPD
13, 14695–14747, 2013

ter, in the BL, CO increases from west to east, suggesting strong contamination by dry CO-polluted air from central and eastern Europe, in agreement with Kaiser (2009). The influence of the Po Bassin's on Vienna might be another source of contamination but it is currently difficult to quantify (Kaiser, 2009); (4) over Vienna, whatever the season, at the surface, the O_3 (CO) is at least 10 ppbv (25–50 ppbv) greater than at the other European sites (not shown), again an evidence of higher pollution.

4.2.3 Middle Eastern and Asian profiles

The seasonal profiles for the Middle East (Eastmed and Uaemi) and Asia (Beijing and Japan) are given on Fig. 9. Interestingly, none of them has the typical seasonal O_3 and CO dichotomy as seen over Europe or the Northern US. For O_3, this is due to: (1) a strong positive summer 1–7 km anomaly over Eastmed; (2) a spring profile closer to autumn-winter than usual over Uaemi above 2 km; (3) strong summer anomalies in Asia. Note the CO horizontal scale change for the 2–15 km over Bejing and Japan, and the 0–2 km over Beijing (by a factor of 6).

Over Middle Eastern sites, very similar winter profiles above 1 km for O_3 and CO suggest a probable common source of variance. Thus, the PTC(O_3) seasonal cycle contrast in winter comparing the two sites (Sect. 4.1.1) is mainly due to z_{DT}. The Eastmed autumn profile is in the same range as Europe, except below 3 km, where the minimum of all the studied sites is reached. At that time and below 3 km, a minimum of O_3 and CO over Uaemi might be related to the sea breezes impact at the surface (Eager et al., 2008) and OH efficiency. Lawrence et al. (2010) reported on the evidence of the broad summertime Middle East O_3 maximum around 400–500 hPa. The authors mentioned this O_3 anomaly is "in contrast to the ozone-depleted Asian airmasses observed in the upper troposphere during MINOS, is not always observed in satellite retrievals (e.g., Fishman et al., 2003; Liu et al., 2006)" and that "the cause of this difference is not yet resolved". Therefore, it seems useful to comment the MOZAIC summer profiles in more detail. At 6 km, on both Middle Eastern sites, the O_3 and CO amounts are similar and O_3 is identical to those of Beijing and greater than in Europe. Above 6 km, the O_3

ACPD
13, 14695–14747, 2013

profiles are still comparable but surprisingly less than Europe or Beijing (by 0.02 DU at 9 km) that suggest STE is probably not the most predominant processes involved. Below 6 km, the O_3 profiles show a marked contrast with: (1) over Eastmed, an intense O_3 maximum within 1–6 km, never reached elsewhere in our study; (2) over Uaemi, a pronounced negative O_3 anomaly (by −0.06 DU at 3 km) with higher amounts of CO (+10 %). The strong O_3 and CO anomalies combined to high level of H_2O (not shown) over Uaemi exclude the impact of predominant STE and probably reveal an intense inflow of sea air and an influence of the remote Indian summer monsoon, in agreement with (Li et al., 2001). Lastly, in spring, the Uaemi O_3 profile is unusually close to autumn and winter profiles, in particular at 3 km. These results are in good agreement with the summer extremes shown on the OMI climatology produced by Ziemke et al. (2011) and with the Persian Gulf region study by Lelieveld et al. (2009). The summer O_3 at 5–7 km agrees well with the model results from Liu et al. (2011) and the study from Lelieveld et al. (2009). Liu et al. (2011) emphasize that the geographic position of the Arabian anticyclone has a major influence on chemical transport. They show that the Middle East mid-tropospheric summer maximum is strongly related to Asian sources of pollution (> 30 %), to local production (23 %) and also to northern USA pollution (> 6 %) transported through the subtropical westerly jet that descends in this area. Over the Zagros Mountains, using spaceborne SAGE II[6] data, Kar et al. (2002) found a CO summer positive anomaly at 7 km over 1985–1990 and 1994–1999 and, in a 2003 spaceborne MOPITT study, argued and explained it by thermal mountain winds venting the boundary layer (Kar et al., 2006). We found a different notable summer positive (negative) CO anomaly on Uaemi within 3–6 km (at 7 km) and not over Eastmed, with the MOZAIC sampling conditions and period. Due to a regional complexity, extensive work is needed to go further on the geographical and seasonal variabilities and we deeply recommend in future studies the addition of the H_2O climatology using MOZAIC/IAGOS to reinforce hypothesis on process involved and air mass origin.

[6]Stratospheric Aerosol and Gas Experiment II.

ACPD
13, 14695–14747, 2013

Over Asia (Fig. 9), a comparison of Japan and Beijing seasonal O_3 profiles reveals that: (1) winter and spring profiles are very similar with a difference of less than 0.01 DU; (2) the autumn Beijing profile exceeds Japan by 0.03 DU (only 0.01 DU) in the BL (at 8 km); (3) the summer Beijing profile exceeds Japan by 0.10 DU (0.02 DU) in the BL (at 8 km); thus in Japan, O_3 at 2 km is reduced to the minimum ever seen whatever the season. Interestingly, up to 4 km, Japan has less CO in all seasons than Beijing, by a factor of 2–8, but, above 4 km, the two profiles are similar ($< 0.2 \times 10^{16}$ mol cm^{-2}), suggesting a common source of variance. The Beijing winter CO maximum is huge, exceeding 30×10^{16} mol cm^{-2} or 1800 ppbv in the BL (Japan is 4.2×10^{16} mol cm^{-2} or 220 ppbv, even less than Vienna). A comparison of the two sites highlights the prevailing wind regimes and the predominant monsoon impact. Both sites show a summer O_3 depletion below 5 km but the monsoon is: (1) less efficient over Beijing, probably due to the high CO (10×10^{16} mol cm^{-2} at the surface) compared to Japan; (2) so intense over Japan that, below 4 km, O_3 summer amounts are less than in winter. The monsoon is the most important and powerful regime for reducing tropospheric O_3 at the hemispheric scale.

The pure tropospheric column and profile climatologies of O_3 and CO presented in this study are complementary, highlighting seasonal variability and vertical anomalies and reinforcing the hypothesis on the processes involved in the northern mid-latitudes. The pure tropospheric profiles obtained here are significantly different from atmospheric profiles above 6 km. The autumn/winter and spring/summer seasonal O_3 dichotomy characterizes the typical seasonal behaviour of the vertical pure tropospheric ozone distribution in the northern mid-latitudes. It characterizes the photochemical activity leading to O_3 production. The CO dichotomy, not so obvious and different from the O_3 dichotomy, is pointed out with a winter/spring maximum and a summer/autumn minimum in the free troposphere. The minimum is related to the higher amounts of OH at that time. We have singled out the monsoon as the most efficient regime for O_3 reduction, with a significant impact at the hemispheric scale in the northern-mid latitudes,

ACPD
13, 14695–14747, 2013

below 6 km. Such a pure tropospheric climatology should be considered as a reference for validation remote-sensing instruments or chemistry-transport model outputs.

4.3 Partial tropospheric columns

Here, we investigate the interest of characterizing z_{Ld}, the altitude from which $\mathrm{PTP}_m(X)$ and $\mathrm{MP}_m(X)$ diverges, to calculate the BL, MT and UT partial tropospheric columns (BLC, MTC and UTC, respectively) for USeast, Germany and Japan.

4.3.1 Divergence between MP and PTP

The limit, z_{Ld}, is defined by month and examples are given on the Fig. 2a. The z_{Ld} varies with the seasons and the sites due to either tropopause altitude variations or the occurrence of stratospheric air detection. The z_{Ld} is higher in summer than in winter and generally higher at southern sites than at northern sites. For example, the 6 km minimum of z_{Ld}, observed in late winter over USlake and USeast, is an indication of high residence frequency of the polar jet stream over these regions and a low tropopause. In August, over USeast the z_{Ld} is 9.5 km, therefore the MT ceiling fixed at 8 km, as used in Zbinden et al. (2006), is not satisfactory. We suggest that it should be replaced by the monthly-varying one, z_{Ld}, defined as the lowest altitude where $\mathrm{MP}_m(\mathrm{O_3})$ differs from $\mathrm{PTP}_m(\mathrm{O_3})$ by 0.001 DU. In this way, UT, the layer between z_{Ld} and z_{DT}, strongly influenced by the stratosphere-troposphere transients, will be more faithfully represented by month.

The z_{Ld} seasonal cycle varies in a 6–12 km range (Fig. 10). Due to low variability of the z_{DT} over Germany, z_{Ld} varies less (6.6–8.1 km) than USeast (6.0–9.5 km) or Japan (6.0–11.9 km). Finally, the UT is thicker in winter than in summer (Fig. 10) and z_{Ld} highlights the lowest winter tropopause position in the northern mid-latitudes. This finding is noteworthy because the seasonality of the deepest stratospheric intrusions, the one that stayed more than 4 days in the troposphere, is characterized by a winter maximum and a summer minimum (Stohl et al., 2003). Finally, as dynamical and photochemical

ACPD
13, 14695–14747, 2013

processes are different in the BL, MT and UT, we give the O_3 and CO partial tropospheric columns over USeast, Germany and Japan (the most documented sites) using either the steady 8 km or a monthly-varying z_{Ld} used as the MT ceiling (Fig. 10). The results are summarized in Table 3. No major change in BL is expected with respect to Zbinden et al. (2006) given that the small variations depend only on the time period update.

4.3.2 BL, MT and UT seasonal cycles

The $\mathrm{BLC}_m(O_3)$, the $\mathrm{MTC}_m(O_3)$, and the $\mathrm{UTC}_m(O_3)$ range from 4.8 to 9.8, 12.1 to 23.8 and 2.2 to 9.9 DU, respectively. Thus, using fully defined MOZAIC tropospheric columns and z_{Ld}, $\mathrm{UTC}_m(O_3)$ are enhanced by 2 DU and show smaller amplitudes than those in Zbinden et al. (2006). Interestingly, the $\mathrm{UTC}_m(O_3)$ maximum is shifted from summer to late winter–early spring. This may be observed even over Germany where the z_{DT} and z_{Ld} variations are the lowest. In August, the use of z_{Ld} over Japan needs to be taken with caution due to the low sampling rate of the upper-tropospheric layers. Besides the $\mathrm{UTC}_m(O_3)$ shift, we also highlight the intense vertical expansion of $\mathrm{MTC}_m(O_3)$. Thus, over Japan, the previous obvious spring $\mathrm{MTC}_m(O_3)$ maximum has turned into a pronounced summer maximum because the O_3-poor air mass due to monsoon in the lower mid-troposphere is balanced by the high column height.

The $\mathrm{BLC}_m(\mathrm{CO})$, the $\mathrm{MTC}_m(\mathrm{CO})$, and the $\mathrm{UTC}_m(\mathrm{CO})$ range from 0.7 to 1.1, 0.9 to 1.4 and 0.1 to 0.6 $\times 10^{18}$ mol cm^{-2}, respectively. The $\mathrm{BLC}_m(\mathrm{CO})$ of the three sites show an increase in amounts and amplitudes from west to east, with a late winter/early spring maximum and a summer minimum.

Even over Germany, where the seasonal z_{DT} is very flat, in MT and UT, the cycles and amplitudes change when the monthly-varying z_{Ld} is used instead of a fixed 8 km altitude. This change becomes significant over USeast and Japan is obviously linked either to the reservoir thickness and the O_3 amounts. The spring O_3 maximum in MT observed using a fixed 8 km altitude has turned into a broad April–August maximum using z_{Ld} and UT has turned out of phase with an overall August minimum and spring maximum.

4.4 Comparison with spaceborne measurements

Our aim, in this last section, is not to validate satellite products but to demonstrate the benefits of such pure tropospheric climatology based on MOZAIC fully-defined individual tropospheric columns. Thus, we compare our new O_3 and CO pure tropospheric columns with the publicly available remote-sensing results from the Giovanni web site (http://disc.sci.gsfc.nasa.gov/giovanni) on a monthly-average basis. The satellite results used for comparison are: the tropospheric O_3 columns from TES[7] (Beer et al., 2001; Worden et al., 2007) by selecting the periods 2006–2007 or 2007 and the CO columns from AIRS[8] (Susskind et al., 2003, 2010). We focus only on two sites because of their contrasting z_{DT} seasonal cycle: Germany [47–52° N, 6–10° E] and Japan (Fig. 11) by providing separately Tokyo [138.7–140.7° N, 35.6–37.6° E], Nagoya [34.1–36.1° N, 135.8–137.8° E] and Osaka [33–35° N, 134–136° E] to check also the consistency of the individual sites.

4.4.1 Ozone

First of all, the recent O_3 tropospheric climatology study from Ziemke et al. (2011) merits consideration. It combines OMI/MLS measurements over six years (2004–2010). Interestingly, on two regions not sampled by ozonesondes, OMI/MLS results in Ziemke et al. (2011) are in agreement with: (1) the MOZAIC tropospheric seasonal cycle over Los Angeles, where the filling of the MOZAIC unvisited tropospheric remainder has modified the seasonal cycle; (2) the largest MOZAIC tropospheric O_3 column in summer (> 40–45 DU) over Eastmed. Nevertheless, the OMI/MLS summer results over

[7]Tropospheric Emission Spectrometer.

[8]Atmospheric InfraRed Sounder.

ACPD
13, 14695–14747, 2013

Japan (Ziemke et al., 2011, Fig. 5b) show a June maximum and remains high in July–August whereas MOZAIC starts a sharp decline.

Although OMI gives global distributions of tropospheric ozone, TES is the first space-borne instrument to provide vertically-resolved information on tropospheric O_3, despite a low sensitivity below 900 hPa (Osterman et al., 2008). For these reasons, we now consider the seasonal cycles of the pure tropospheric O_3 derived from MOZAIC and the tropospheric results from TES (Fig. 11, left). Over Germany, the correlation is excellent ($r = 0.93$) with a TES positive bias by 9–14 DU. The O_3 seasonal cycles (Fig. 11, top left) are well phased with a summer maximum and a winter minimum. Interestingly, larger winter TES positive bias, by 2–3 DU, are visible. Over Japan, a strong May maximum is observed on both cycles, and an additional secondary winter maximum is detected by TES. Consequently, the correlation drops to $r = 0.60$–0.76, with a TES positive bias of 9–18 DU. These results are consistent with, but all higher than the 7 DU (2.8 DU) bias found by comparing TES tropospheric columns (by adding the averaging kernel) with 1425 sondes, as reported by Osterman et al. (2008). Herman and Osterman (2011) have reported that the "TES ozone profiles are positively biased (by less than 15 %) from the surface to the upper-troposphere (from ∼ 1000 to 100 hPa) and negatively biased (by less than 20 %) from the upper troposphere to the lower stratosphere (from 100 to 30 hPa) when compared to the ozone-sonde data". Thus, beside the bias due to the instrument vertical resolution and/or the retrieval technique (not discussed here) the differences between MOZAIC and TES are reinforced because: (1) the observation time influences the O_3 measured in the BL: TES orbit is sun-synchronous with a 13:43 local time (LT) ascending node, comparable to OMI/MLS, while MOZAIC depends on commercial aircraft schedules. The 0–2 km partial column difference in the seasonal cycle using MOZAIC observations over Frankfurt selected at 02:00–06:00 and 11:00–18:00 LT is evaluated to be 2 DU maximum (not shown). (2) MOZAIC is almost insensitive to hydrometeorological conditions while TES data processing requires cloud screening, thus introducing a probable bias due to specific meteorological conditions of sampling. Nonetheless, how can such enlarged winter in-

ACPD
13, 14695–14747, 2013

situ and spaceborne differences (> 3 DU) be explained at those two sites? In winter, the BL and MT have the lowest O_3 contributions (Fig. 10, top) and z_{DT} is at a minimum. This suggests that the tropopause positioning makes the main contribution to the winter differences, probably because of the 6–7 km vertical resolution of TES measurements and that the tropospheric ozone column might contain some stratospheric information as reported by Osterman et al. (2008). We agree with Stajner et al. (2008), who emphasize the impact of tropopause location on tropospheric O_3 columns, interannual variability and trend estimates. An insufficient accuracy on the characterization of the tropopause altitude leads to strong stratospheric contamination in the pure tropospheric O_3 reservoir (Fig. 2) and thus may impact the assessment of trends in th UT.

4.4.2 Carbon monoxide

The AIRS seasonal cycles of total columns and our pure tropospheric seasonal cycles are correlated by $r = 0.89$ ($r = 0.80$) on the descending (ascending) node over Germany. They show a larger difference in winter and a similar response at the summer minimum (Fig. 11, right). As the CO maximum along the vertical is below 2 km and as the impact of tropopause height is negligible, the winter difference may be explained by the weak sensitivity of the satellite instrument in the BL. The winter maximum is clearly not well captured by AIRS. Diurnal variations are zero from July to January and maximum in April. Considering Japan, the correlations are $r = 0.96$–0.98 on the ascending node (13:00 LT) and $r = 0.93$–0.97 on descending node (07:00 LT). From AIRS, we observe differences on the diurnal CO cycle, which are larger in winter-spring and almost zero in summer. They also show a west to east negative gradient between the individual Japanese airports. In summer, note the best agreement over Germany and the excellent agreement between our pure tropospheric seasonal cycles and AIRS at that season. The differences may be due to less thermal contrast between air in the lower boundary layer and in the surface layer. Besides the low AIRS sensitivity in the BL,

ACPD
13, 14695–14747, 2013

an additional source of differences is the cloud screening, a mandatory constraint for AIRS but not required for MOZAIC inducing a sampling effect in the intercomparison.

5 Conclusions

A new and comprehensive O_3 and CO pure tropospheric climatology has been derived from MOZAIC over 1994–2009 including 40 000 profiles. Eleven sites were documented between 24–50° N and from Los Angeles to Japan to give a quasi global picture of the northern-mid-latitudes. The previous low-biased tropospheric O_3 climatology (Zbinden et al., 2006) has been improved by adding the complete estimate of the MOZAIC unvisited tropospheric remainder, and CO. The outcome is a fully defined pure tropospheric climatology from the ground to the individual dynamical tropopause based solely on the MOZAIC individual profiles. The O_3 validation was performed using composite results derived from time-coincident MOZAIC profiles and WOUDC soundings close to the most documented MOZAIC sites (USeast, Germany, Japan). The pure O_3 tropospheric columns reproduce 96–98 % of the composite tropospheric columns after the addition of WOUDC partial columns to MOZAIC when necessary. Therefore, the pure tropospheric profiles (by season) and columns (by month) are the most robust and accurate vertically-integrated results based on in-situ measurements. As far as we know, this is the first pure tropospheric climatology and is significantly different from climatological profiles at all the sites, as seen in particular for ozone or by referring to Logan (1994); McPeters et al. (2007); Stajner et al. (2008); Ding et al. (2008) and Tilmes et al. (2012).

The first outcome is that the seasonal cycles of the pure tropospheric columns are in the range of 23.7–43.2 DU for O_3 and $1.5–6.8 \times 10^{18}$ mol cm^{-2} for CO. Due to the photochemistry and OH removal efficiency, the maxima of the seasonal cycles are not in phase: February–April for CO, May–July for O_3. In terms of zonal variability, for O_3 we globally observe greater summer contents over the northern US, the lowest contents whatever the months considered over Europe and the greatest spring and summer contents in the Middle East and Beijing. The summer Asian monsoon results in a sharp decrease over Japan, not observed over Beijing, and, surprisingly, in a weakened maximum over Uaemi. In addition, Los Angeles appears more connected to Asia than to any other site excepted in summer. For CO, the Beijing minimum exceeds the maxima of all other sites for all seasons. The smallest amplitudes and the lowest winter–spring CO columns are detected in the Middle East.

The second outcome is the seasonal pure tropospheric profile climatology. At all sites, the O_3 pure tropospheric profiles, in DU, never return to a positive vertical gradient above 2 km (except on the poorly sampled winter profiles of Los Angeles), unlike the monthly-averaged MOZAIC O_3 profiles. The spring-summer/autumn-winter seasonal dichotomy on O_3 seasonal profiles is confirmed, as is the deep summer decrease due to the monsoon over Japan, Beijing and USsouth with different intensities. Comparing Uaemi with Eastmed in summer, a strong negative O_3 anomaly below 6 km appears. It could be linked to the impact of sea breeze or depleted maritime air inflow from regions under Indian monsoon conditions. Regarding CO, we observe a summer-autumn/winter-spring dichotomy with a clear winter maximum in the BL. Note that, in the BL, the CO winter maximum over Beijing is 2–7 times (2–6 times) greater than over Japan (Europe), whereas only twice above 5 km. Additionally, comparing all the sites in winter at 5 km for CO, the minimum is encountered over the Middle East and South–Western US sites, while North–Eastern US sites and Europe show comparable and higher amounts in contrast with the strong Asian maximum values. The vertical profile study shows a large O_3 and CO homogeneity among the European sites with a west to east gradient. We found the upper pure tropospheric layers to be very consistent among chemical species, namely with less O_3 and more CO than when tropospheric/stratospheric reservoirs were undifferentiated, even if monthly-averaged profiles were limited to the monthly-averaged tropopause altitude.

As the third outcome, we provide the seasonal cycles of the BL, MT and UT partial columns using a new monthly-varying criterion, L_d, as the MT ceiling, because of their distinct predominant processes. Consequently, the tropopause of all individual

ACPD
13, 14695–14747, 2013

profiles within the time-series will always be above L_d and thus UT is more faithfully represented. The L_d is detected at 6–12 km on overage, with a winter minimum and summer maximum. This approach highlights a predominant increase (decrease) in the MT O_3 amount associated with a summer (winter) wide MT thickening (thinning). The UT O_3 seasonal cycle, maximized earlier than when a fixed ceiling was used, is now more comparable to the UT O_3 seasonal cycle defined using a tropopause reference (Thouret et al., 2006). For CO, it is interesting to note that the clear MT spring maximum is shifted to a broad April–August maximum, in contrast to what happens in the UT.

Last outcome highlight the benefits of this pure tropospheric climatology based on in-situ measurements by comparing the seasonal cycles of the MOZAIC tropospheric columns with those derived from satellites. We focused on two sites, Germany and Japan, because of their contrasting tropopause altitude and seasonal variability. We found consistent seasonal cycles from MOZAIC and satellite data, although with noteworthy differences: (1) for O_3, TES tropospheric columns are correlated with MOZAIC by $r = 0.6$ (Japan) and $r = 0.9$ (Germany), are greater than MOZAIC by 9–18 DU, and the largest biases occur in winter; (2) for CO, AIRS total columns provide a response as much as 1.0×10^{18} mol cm^{-2} lower than MOZAIC ($r > 0.9$). Besides the instrumental bias, the tropopause is a probable source of discrepancy because just below the monthly tropopause, the MOZAIC profile $MP_m(O_3)$ exceeds our fully defined and pure tropospheric profile. We noted a greater O_3 bias in winter, when the tropopause is low (2–3 DU over Germany, > 5 DU over Japan). Therefore, the O_3 difference is probably mostly explained by stratospheric air contamination but also by clear sky conditions or the satellite overpass-time capturing the daily maximum. All three factors can enhance the satellite response. We point out the need of an accurate discrimination between the stratospheric and tropospheric reservoirs, and indeed the monthly tropopause is an unappropriated criteria. This point is crucial, merits consideration and has to be clarified in the framework of tropospheric trends and radiative transfer studies.

ACPD
13, 14695–14747, 2013

These fully defined and pure tropospheric products will be available in the MOZAIC/IAGOS database to the scientific community. Such climatologies will be regularly updated thanks to the on-going MOZAIC programme, IAGOS, on the associated data base http://www.iagos.org/.

Acknowledgements. The authors gratefully acknowledge F. Karcher deeply involved in the MOZAIC/IAGOS program. Acknowledgements are adressed for to the European Commission their strong support and to Airbus, and the airlines (Lufthansa, Austrian, Air France) who have carried the MOZAIC equipment and performed the maintenance free of charge since 1994. MOZAIC is presently funded by INSU-CNRS (France), Météo-France, and Forschungszentrum (FZJ, Jülich, Germany) and data base is supported by ETHER (CNES and INSU-CNRS). We also thank the German Weather Service (Meteorological Observatory at Hohenpeissenberg), the National Space Development Agency of Japan and NASA (Wallops Island Flight Facility) for providing their data through the World Ozone and Ultraviolet Radiation Data Centre (WOUDC) operated by Environment Canada, Toronto, Ontario, Canada, under the auspices of the World Meteorological Organization. The remote sensing data were acquired as part of NASA's Earth-Sun System Division and archived and distributed by the Goddard Earth Sciences (GES) Data and Information Services Center (DISC) Distributed Active Archive Center (DAAC). We acknowledge the mission scientists and Principal Investigators who provided the TES and AIRS data used in this research through the Giovanni web site (http://disc.sci.gsfc.nasa.gov/giovanni/).

The publication of this article is financed by CNRS-INSU.

References

Aghedo, A. M., Bowman, K. W., Worden, H. M., Kulawik, S. S., Shindell, D. T., Lamarque, J. F., Faluvegi, G., Parrington, M., Jones, D. B. A., and Rast, S.: The vertical distribution of ozone instantaneous radiative forcing from satellite and chemistry climate models, J. Geophys. Res., 116, D01305, doi:10.1029/2010JD014243, 2011. 14697

Agusti-Panareda, A., Gray, S. L., and Methven, J.: Numerical modelling study of boundary-layer ventilation by a cold front over Europe, J. Geophys. Res., 110, D18304, doi:10.1029/2004JD005555, 2005. 14697

Auvray, M. and Bey, I.: Long-range transport to Europe: seasonal variations and implications for the European ozone budget, J. Geophys. Res., 110, D11303, doi:10.1029/2004JD005503, 2005. 14697

Baumann, K., Maurer, H., Rau, G., Piringer, M., Pechinger, U., Prévôt A., Furgerb, M., Neiningerc, B., and Pellegrini, U.: The influence of south Foehn on the ozone distribution in the Alpine Rhine valley – results from the MAP field phase, Atmos. Environ., 35, 6379–6390, doi:10.1016/S1352-2310(01)00364-8, 2001. 14706

Beer, R., Glavich, T. A., and Rider, D. M.: Tropospheric emission spectrometer for the Earth Observing System's Aura Satellite, Appl. Optics, 40, 2356–2367, 2001. 14719

Brown-Steiner, B. and Hess, P.: Asian influence on surface ozone in the United States: a comparison of chemistry, seasonality, and transport mechanisms, J. Geophys. Res., 116, D17309, doi:10.1029/2011JD015846, 2011. 14707

Clerbaux, C., George, M., Turquety, S., Walker, K. A., Barret, B., Bernath, P., Boone, C., Borsdorff, T., Cammas, J. P., Catoire, V., Coffey, M., Coheur, P.-F., Deeter, M., De Mazière, M., Drummond, J., Duchatelet, P., Dupuy, E., de Zafra, R., Eddounia, F., Edwards, D. P., Emmons, L., Funke, B., Gille, J., Griffith, D. W. T., Hannigan, J., Hase, F., Höpfner, M., Jones, N., Kagawa, A., Kasai, Y., Kramer, I., Le Flochmoën, E., Livesey, N. J., López-Puertas, M., Luo, M., Mahieu, E., Murtagh, D., Nédélec, P., Pazmino, A., Pumphrey, H., Ricaud, P., Rinsland, C. P., Robert, C., Schneider, M., Senten, C., Stiller, G., Strandberg, A., Strong, K., Sussmann, R., Thouret, V., Urban, J., and Wiacek, A.: CO measurements from the ACE-FTS satellite instrument: data analysis and validation using ground-based, airborne and spaceborne observations, Atmos. Chem. Phys., 8, 2569–2594, doi:10.5194/acp-8-2569-2008, 2008. 14709

Cooper, O. R., Stohl, A., Eckhardt, S., Parrish, D. D., Oltmans, S. J., Johnson, B. J., Nédélec P., Schmidlin, F. J., Newchurch, M. J., Kondo, Y., Kita, K.: A springtime comparison of tropospheric ozone and transport pathways on the east and west coasts of the United States, J. Geophys. Res., 110, D05S90, doi:10.1029/2004JD005183, 2005. 14713

Cooper, O. R., Stohl, A., Trainer, M., Thompson, A. M., Witte, J. C., Oltmans, S. J., Morris, G., Pickering, K. E., Crawford, J. H., Chen, G., Cohen, R. C., Bertram, T. H., Wooldridge, P., Perring, A., Brune, W. H., Merrill, J., Moody, J. L., Tarasick, D., Nédélec P., Forbes, G., Newchurch, M. J., Schmidlin, F. J., Johnson, B. J., Turquety, S., Baughcum, S. L., Ren, X., Fehsenfeld, F. C., Meagher, J. F., Spichtinger, N., Brown, C. C., McKeen, S. A., McDermid, I. S., and Leblanc, T.: Large upper tropospheric ozone enhancements above midlatitude North America during summer: in situ evidence from the IONS and MOZAIC ozone measurement network, J. Geophys. Res., 111, D24S05, doi:10.1029/2006JD007306, 2006. 14707, 14708, 14713

Cooper, O. R., Parrish, D. D., Stohl, A., Trainer, M., Nédélec P., Thouret, V., Cammas, J. P., Oltmans, S. J., Johnson, B. J., Tarasick, D., Leblanc, T., McDermid, I. S., Jaffe, D., Gao, R., Stith, J., Ryerson, T., Aikin, K., Campos, T., Weinheimer, A., and Avery, M. A.: Increasing springtime ozone mixing ratios in the free troposphere over western North America, Nature, 463, 344–348, doi:10.1038/nature08708, 2010. 14697, 14707

Danielsen, E. F.: Stratospheric-tropospheric exchange based on radioactivity, ozone and potential vorticity, J. Atmos. Sci., 25, 502–528, 1968. 14697

Ding, A. J., Wang, T., Thouret, V., Cammas, J.-P., and Nédélec, P.: Tropospheric ozone climatology over Beijing: analysis of aircraft data from the MOZAIC program, Atmos. Chem. Phys., 8, 1–13, doi:10.5194/acp-8-1-2008, 2008. 14722

Eager, R. E., Raman, S., Wootten, A., Westphal, D. L., Reid, J. S., and Al Mandoos, A.: A climatological study of the sea and land breezes in the Arabian Gulf region, J. Geophys. Res., 113, D15106, doi:10.1029/2007JD009710, 2008. 14714

Emmons, L. K., Deeter, M. N., Gille, J. C., Edwards, D. P., Attié J.-L., Warner, J., Ziskin, D., Francis, G., Khattatov, B., Yudin, V., Lamarque, J.-F., Ho, S.-P., Mao, D., Chen, J. S., Drummond, J., Novelli, P., Sachse, G., Coffey, M. T., Hannigan, J. W., Gerbig, C., Kawakami, S., Kondo, Y., Takegawa, N., Schlager, H., Baehr, J., and Ziereis, H.: Validation of Measurements Of Pollution In The Troposphere (MOPITT) CO retrievals with aircraft in situ profiles, J. Geophys. Res., 109, D03309, doi:10.1029/2003JD004101, 2004. 14710

Emmons, L. K., Pfister, G. G., Edwards, D. P., Gille, J. C., Sachse, G., Blake, D., Wofsy, S., Gerbig, C., Matross, D., and Nédélec P., Measurements of Pollution in the Troposphere (MOPITT) validation exercises during summer 2004 field campaigns over North America, J. Geophys. Res., 112, D12S02, doi:10.1029/2006JD007833, 2007. 14710

Emmons, L. K., Edwards, D. P., Deeter, M. N., Gille, J. C., Campos, T., Nédélec P., Novelli, P., and Sachse, G.: Measurements Of Pollution In The Troposphere (MOPITT) validation through 2006, Atmos. Chem. Phys., 9, 1795–1803, 2009, http://www.atmos-chem-phys.net/9/1795/2009/. 14710

Felzer, B. S., Cronin, T., Reilly, J. M., Melillo, J. M., and Wang, X.: Impacts of ozone on trees and drops, C. R. Geosci., 339, 784–798, doi:10.1016/j.crte.2007.08.008, 2007. 14697

Fishman, J. and Larsen, J. C.: Distribution of tropospheric ozone determined from satellite data, J. Geophys. Res., 95, 3599–3617, 1990. 14697

Forster de P. M., and Shine, K. P.: Radiative forcing and temperature trends from stratospheric ozone changes, J. Geophys. Re., 102, 10841–10855, 1997. 14697

Guttikunda, S. K., Tang, Y., Carmichael, G. R., Kurata, G., Pan, L., Streets, D. G., Woo, J.-H., Thongboonchoo, N., and Fried, A.: Impacts of Asian megacity emissions on regional air quality during spring 2001, J. Geophys. Res., 110, D20301, doi:10.1029/2004JD004921, 2005. 14697

Hegglin, M. I., Boone, C. D., Manney, G. L., Shepherd, T. G., Walker, K. A., Bernath, P. F., Daffer, W. H., Hoor, P., and Schiller, C.: Validation of ACE-FTS satellite data in the upper troposphere/lower stratosphere (UTLS) using non-coincident measurements, Atmos. Chem. Phys., 8, 1483–1499, doi:10.5194/acp-8-1483-2008, 2008. 14709

Herman, R. and Osterman, G.: Earth Observing System (EOS) Tropospheric Emission Spectrometer (TES) Data Validation Report (Version F05_05, F05_06, F05_07 data), Jet Propulsion Laboratory, California Institute of Technology, Pasadena, California, 99 pp., 23 November 2011. 14720

Hoskins, B. J., McIntyre, M. E., and Robertson, A. W. On the use and significance of isentropic potential vorticity maps, Quaterly J. Meteorol. Soc., 111, 877–946, 1985. 14699

Jaffe, D. and Ray, J.: Increase in surface ozone at rural sites in the western US, Atmos. Environ., 41, 5452–5463, doi:10.1016/j.atmosenv.2007.02.034, 2007. 14707

Jaffe, D., Price, H., Parrish, D., Goldstein, A., and Harris, J.: Increasing background ozone during spring on the west coast of North America, Geophys. Res. Lett., 30, 1613, doi:10.1029/2003GL017024, 2003. 14707, 14713

Junge, C. E.: Global ozone budget and exchange between stratosphere and troposphere, Tellus, 14, 363–377, 1962. 14697

Kar, J., Trepte, C. R., Thomason, L. W., Zawodny, J. M., Cunnold, D. M., and Wang, H. J.: On the tropospheric mequrements of ozone by the Stratospheric Aerosol and Gas

Experiment II (Sage II, version 6.1) in the tropics, Geophys. Res. Lett., 29, 2208, doi:10.1029/2002GL016241, 2002. 14715

Kar, J., Drummond, J. R., Jones, D. B. A., Liu, J., Nichitiu, F., Zou, J., Gille, J. C., Edwards, D. P., and Deeter, M. N.: Carbon monoxide (CO) maximum over the Zagros mountains in the Middle East: Signature of mountain venting?, Geophys. Res. Lett., 33, L15819, doi:10.1029/2006GL026231, 2006. 14715

Kaiser, A.: Origin of polluted air masses in the Alps. An overview and first results for MONARPOP, Environ. Pollut., 157, 3232–3237, doi:10.1016/j.envpol.2009.05.042, 2009. 14714

Lamsal, L. N., Martin, R. V., Padmanabhan, A., van Donkelaar, A., Zhang, Q., Sioris, C. E., Chance, K., Kurosu, T. P., and Newchurch, M. J.: Application of satellite observations for timely updates to global anthropogenic NO_x emission inventories, Geophys. Res. Lett., 38, L05810, doi:10.1029/2010GL046476, 2011. 14707, 14711

Lawrence, M. G. and Lelieveld, J.: Atmospheric pollutant outflow from southern Asia: a review, Atmos. Chem. Phys., 10, 11017–11096, doi:10.5194/acp-10-11017-2010, 2010. 14714

Lelieveld, J., Hoor, P., Jöckel, P., Pozzer, A., Hadjinicolaou, P., Cammas, J.-P., and Beirle, S.: Severe ozone air pollution in the Persian Gulf region, Atmos. Chem. Phys., 9, 1393–1406, doi:10.5194/acp-9-1393-2009, 2009. 14715

Li, Q., Jacob, D. J., Logan, J. A., Bey, I., Yantosca, R. M., Liu, H., Martin, R. V., Fiore, A. M., Field, B. D., and Duncan, B. N.: A tropospheric ozone maximum over the Middle East, Geophys. Res. Lett., 28, 3235–3238, 2001. 14715

Li, Q., Jacob, D. J., Park, R., Wang, Y., Heald, C. L., Hudman, R., Yantosca, R. M., Martin, R. V., and Evans, M.: North American pollution outflow and the trapping of convectively lifted pollution by upper-level anticyclone, J. Geophys. Res., 110, D10301, doi:10.1029/2004JD005039, 2005. 14708, 14710, 14713

Liu, J., Drummond, J. R., Jones, D. B. A., Cao, Z., Bremer, H., Kar, J., Zou, J., Nichitiu, F., and Gille, J. C.: Large horizontal gradients in atmospheric CO at the synoptic scale as seen by spaceborne Measurements of Pollution in the Troposphere, J. Geophys. Res., 111, D02306, doi:10.1029/2005JD006076, 2006. 14710

Liu, J., Jones, D. B. A., Zhang, S., and Kar, J.: Influence of interannual variations in transport on summertime abundances of ozone over the Middle East, J. Geophys. Res., 116, D20310, doi:10.1029/2011JD016188, 2011. 14715

Logan, J.: Tropospheric ozone seasonal behavior, trends, and anthropogenic influence, J. Geophys. Res., 90, 10463–10482, 1985. 14697, 14707

ACPD
13, 14695–14747, 2013

Pure Tropospheric O_3 and CO profiles and columns contents

R. M. Zbinden et al.

Logan, J.: Trends in the vertical distribution of ozone: an analysis of ozonesonde data, J. Geophys. Res., 94, 25553–25585, 1994. 14697, 14722

Logan, J.: An analysis of ozonesonde data for the troposphere: recommendations for testing 3-D models and development of a gridded climatology for tropospheric ozone, J. Geophys. Res., 104, 16115–16149, 1999. 14697, 14707

McPeters, R. D., Labow, G. J., and Logan, J. A.: Ozone climatological profiles for satellite retrieval algorithms, J. Geophys. Res., 112, D05308, doi:10.1029/2005JD006823, 2007. 14722

Marenco, A., Thouret, V., Nédélec P., Smit, H., Helten, M., Kley, D., Karcher, F., Simon, P., Law, K., Pyle, J., Poschmann, G., Von Wrede, R., Hume, C., Cook, T.: Measurement of ozone and water vapor by Airbus in-service aircraft: the MOZAIC airborne program, an overview, J. Geophys. Res., 103, 631–642, 1998. 14697, 14698

Nedelec, P., Cammas, J.-P., Thouret, V., Athier, G., Cousin, J.-M., Legrand, C., Abonnel, C., Lecoeur, F., Cayez, G., and Marizy, C.: An improved infrared carbon monoxide analyser for routine measurements aboard commercial Airbus aircraft: technical validation and first scientific results of the MOZAIC III programme, Atmos. Chem. Phys., 3, 1551–1564, doi:10.5194/acp-3-1551-2003, 2003. 14699

Neuman, J. A., Trainer, M., Aikin, K. C., Angevine, W. M., Brioude, J., Brown, S. S., de Gouw, J. A., Dube, W. P., Flynn, J. H., Graus, M., Holloway, J. S., Lefer, B. L., Nedelec, P., Nowak, J. B., Parrish, D. D., Pollack, I. B., Roberts, J. M., Ryerson, T. B., Smit, H., Thouret, V., Wagner, N. L.: Observations of ozone transport from the free troposphere to the Los Angeles basin, J. Geophys. Res., 117, D00V09, doi:10.1029/2011JD016919, 2012. 14713

Oltmans, S. J., Lefohn, A. S., Harris, J. M., and Shadwick, D. S.: Background ozone levels of air entering the west coast of the US and assessment of longer-term changes, Atmos. Environ., 42, 6020–6038, 2008. 14708, 14713

Osterman, G. B., Kulawik, S. S., Worden, H. M., Richards, N. A. D., Fisher, B. M., Eldering, A., Shephard, M. W., Froidevaux, L., Labow, G., Luo, M., Herman, R. L., Bowman, K. W., and Thompson, A. M.: Validation of Tropospheric Emission Spectrometer (TES) measurements of the total, stratospheric, and tropospheric column abundance of ozone, J. Geophys. Res., 113, D15S16, doi:10.1029/2007JD008801, 2008. 14720, 14721

Parrish, D., Dunlea, E. J., Atlas, E. L., Schauffler, S., Donnelly, S., Stroud, V., Goldstein, A. H., Millet, D. B., McKay, M., Jaffe, D. A., Price, H. U., Hess, P. G., Flocke, F., and Roberts, J. M.: Changes in the photochemical environment of the temperate North Pacific

ACPD
13, 14695–14747, 2013

Pure Tropospheric O_3 and CO profiles and columns contents

R. M. Zbinden et al.

troposphere in response to increased Asian emissions, J. Geophys. Res., 109, D23S18, doi:10.1029/2004JD004978, 2004. 14707, 14713

Riese, M., Ploeger, F., Rap, A., Vogel, B., Konopka, P., Dameris, M., Forster, P.: Impact of uncertainties in atmospheric mixing on simulated UTLS composition and related radiative effects, J. Geophys. Res., 117, D16305, doi:10.1029/2012JD017751, 2012. 14697

Schneider, P. and van der A, R. J.: A global single-sensor analysis of 2002–2011 tropospheric nitrogen dioxide trends observed from space J. Geophys. Res., 117, D16309, doi:10.1029/2012JD017571, 2012. 14711

Stajner, I., Wargan, K., Pawson, S., Hayashi, H., Chang, L.-P., Hudman R. C., Froidevaux, L., Livesey, N., Levelt, P. F., Thompson, A. M., Tarasick, D. W., Stübi R., Andersen, S. B., Yela, M., König-Langlo, G., Schmidlin, F. J., and Witte, J. C.: Assimilated ozone from EOS-Aura: evaluation of the tropopause region and tropospheric columns, J. Geophys. Res., 113, D16S32, doi:10.1029/2007JD008863, 2008. 14721, 14722

Stohl, A., Bonasoni, P., Cristofanelli, P., Collins, W., Feichter, J., Frank, A., Forster, C., Gerasopoulos, E., Gäggeler H., James, P., Kentarchos, T., Kromp-Kolb, H., Krüger B., Land, C., Meloen, J., Papayannis, A., Priller, A., Seibert, P., Sprenger, M., Roelofs, G. J., Scheel, H. E., Schnabel, C., Siegmund, P., Tobler, L., T. Trickl, T., Wernli, H.,Wirth, V., Zanis, P., and Zerefos, C.: Stratosphere-troposphere exchange: a review and what we have learned from STACCATO, J. Geophys. Res., 108, 8516, doi:10.1029/2002JD002490, 2003. 14697, 14717

Susskind, J., Barnet, C. D., and Blaisdell, J. M.: Retrieval of atmospheric and surface parameters from AIRS/AMSU/HSB Data in the presence of clouds, IEEE T. Geosci. Remote, 41, 2, 390–409, doi:10.1109/TGRS.2002.808236, 2003. 14719

Susskind, J., Blaisdell, J., and Rosenkranz, P.: AIRS/AMSU/HSB Version 5 Level 2 Quality Control and Error Estimation Ed: E. T. Olsen Version 1.1 Jet Propulsion Laboratory, California Institute of Technology, Pasadena, CA, USA, 15 pp., March 2010. 14719

Tangborn, A., Stajner, I., Buchwitz, M., Khlystova, I., Pawson, S., Burrows, J., Hudman, R., and Nédélec P.: Assimilation of SCIAMACHY total column CO observations: global and regional analysis of data impact, J. Geophys. Res., 114, D07307, doi:10.1029/2008JD010781, 2009. 14711

Thouret, V., Marenco, A., Logan, J. A., Nédélec P., and Grouhel, C.: Comparisons of ozone measurements from the MOZAIC airborne program and the ozone sounding network at eight locations, J. Geophys. Res., 103, 695–720, 1998. 14698

ACPD
13, 14695–14747, 2013

Pure Tropospheric O_3 and CO profiles and columns contents

R. M. Zbinden et al.

Thouret, V., Cammas, J.-P., Sauvage, B., Athier, G., Zbinden, R., Nédélec, P., Simon, P., and Karcher, F.: Tropopause referenced ozone climatology and inter-annual variability (1994–2003) from the MOZAIC programme, Atmos. Chem. Phys., 6, 1033–1051, doi:10.5194/acp-6-1033-2006, 2006. 14699, 14700, 14724

Tilmes, S., Lamarque, J.-F., Emmons, L. K., Conley, A., Schultz, M. G., Saunois, M., Thouret, V., Thompson, A. M., Oltmans, S. J., Johnson, B., and Tarasick, D.: Technical Note: Ozonesonde climatology between 1995 and 2011: description, evaluation and applications, Atmos. Chem. Phys., 12, 7475–7497, doi:10.5194/acp-12-7475-2012, 2012. 14722

Turquety, S., Logan, J. A., Jacob, D. J., Hudman, R. C., Leung, F. Y., Heald, C. L., Yantosca, R. M., Wu, S., Emmons, L. K., Edwards, D. P., Sachse, G. W.: Inventory of boreal fire emissions for North America in 2004: Importance of peat burning and pyroconvective injection, J. Geophys. Res., 112, D12S03, doi:10.1029/2006JD007281, 2007. 14710

van der A, R. J., Eskes, H. J., Boersma, K. F., van Noije, T. P. C., Van Roozendael, M., De Smedt, I., Peters, D. H. M. U., and Meijer, E. W.: Trends, seasonal variability and dominant NO_x source derived from a ten year record of NO_2 measured from space, J. Geophys. Res., 113, D04302, doi:10.1029/2007JD009021, 2008. 14711

Wang, Y., Konopka, P., Liu, Y., Chen, H., Müller, R., Plöger, F., Riese, M., Cai, Z., and Lü, D.: Tropospheric ozone trend over Beijing from 2002–2010: ozonesonde measurements and modeling analysis, Atmos. Chem. Phys., 12, 8389–8399, doi:10.5194/acp-12-8389-2012, 2012. 14707

Wernli, H. and Bourqui, M.: A Lagrangian "one-year climatology" of (deep) cross-tropopause exchange in the extratropical Northern Hemisphere, J. Geophys. Res., 107, 4021, doi:10.1029/2001JD000812, 2002. 14697

West, J. J., Szopa, S., and Hauglustaine, D. A.: Human mortality effects of future concentrations of tropospheric ozone, C. R. Geosci., 339, 775–783, doi:10.1016/j.crte.2007.08.005, 2007. 14697

Worden, H. M., Logan, J. A., Worden, J. R., Beer, R., Bowman, K., Clough, S. A., Eldering, A., Fisher, B. M., Gunson, M. R., Herman, R. L., Kulawik, S. S., Lampel, M. C., Luo, M., Megretskaia, I. A., Osterman, G. B., and Shephard, M. W.: Comparisons of Tropospheric Emission Spectrometer (TES) ozone profiles to ozonesondes: methods and initial results, J. Geophys. Res.-Atmos., 112, D03309, doi:10.1029/2006JD007258, 2007. 14719

Yurganov, L. N., Blumenstock, T., Grechko, E. I., Hase, F., Hyer, E. J., Kasischke, E. S., Koike, M., Kondo, Y., Kramer, I., Leung, F.-Y., Mahieu, E., Mellqvist, J., Notholt, J., Nov-

ACPD
13, 14695–14747, 2013

Pure Tropospheric O_3 and CO profiles and columns contents

R. M. Zbinden et al.

elli, P. C., Rinsland, C. P., Scheel, H. E., Schulz, A., Strandberg, A., Sussmann, R., Tanimoto, H., Velazco, V., Zander, R., and Zhao, Y.: A quantitative assessment of the 1998 carbon monoxide emission anomaly in the Northern Hemisphere based on total column and surface concentration measurements, J. Geophys. Res., 109, D15305, doi:10.1029/2004JD004559, 2004. 14697

Zbinden, R. M., Cammas, J.-P., Thouret, V., Nédélec, P., Karcher, F., and Simon, P.: Mid-latitude tropospheric ozone columns from the MOZAIC program: climatology and interannual variability, Atmos. Chem. Phys., 6, 1053–1073, doi:10.5194/acp-6-1053-2006, 2006. 14698, 14699, 14700, 14701, 14702, 14703, 14705, 14712, 14717, 14718, 14722, 14736

Ziemke, J. R., Chandra, S., Labow, G. J., Bhartia, P. K., Froidevaux, L., and Witte, J. C.: A global climatology of tropospheric and stratospheric ozone derived from Aura OMI and MLS measurements, Atmos. Chem. Phys., 11, 9237–9251, doi:10.5194/acp-11-9237-2011, 2011. 14708, 14715, 14719, 14720

ACPD

13, 14695–14747, 2013

Pure Tropospheric O_3 and CO profiles and columns contents

R. M. Zbinden et al.

Table 1. Geographical context of the study over four continents (col 1) with the MOZAIC site labelling (col 2), the related airport or airports for a cluster (col 3), the airport geographic coordinates (col 4), the number of associated MOZAIC profiles (Nb P, col 5), the airport elevation (col 6) and total number of MOZAIC profiles included in this study (bottom line).

Continent	Site label	airport or cluster	Geographic coordinates	Nb P	Elevation (m a.s.l.)
	Los Angeles	Los Angeles	[118.17° W, 34.00° N]	300	38
North America	USeast	Washington, New York, Boston	[77.00° W, 38.92° N], [73.63° W, 40.67° N], [71.00° W, 42.50° N]	5054	5, 4, 6
	USlake	Chicago, Detroit, Toronto	[87.60° W, 41.75° N], [83.34° W, 42.21° N], [79.00° W, 43.00° N]	2425	204, 196, 173
	USsouth	Dallas, Houston	[96.80° W, 32.80° N], [95.25° W, 29.45° N]	2315	185, 30
	Paris	Paris	[2.58° E, 49.00° N]	4379	119
Europe	Germany	Frankfurt, Munich	[9.00° E, 50.00° N], [11.78° E, 48.34° N]	16 041	111, 453
	Vienna	Vienna	[16.37° E, 48.20° N]	4765	183
Middle	Eastmed	Cairo, Tel Aviv	[31.39° E, 30.10° N], [34.89° E, 32.00° N]	702	116, 41
East	Uaemi	Abu Dhabi, Dubai	[54.64° E, 24.44° N], [55.35° E, 25.26° N]	953	27, 19
Asia	Beijing	Beijing	[111.50° E, 40.00° N]	906	35
	Japan	Osaka, Nagoya, Tokyo	[135.00° E, 34.00° N], [136.80° E, 35.10° N], [139.70° E, 35.60° N]	3098	11, 14, 43
			Total Nb of profiles	**40 938**	

ACPD
13, 14695–14747, 2013

Pure Tropospheric O_3 and CO profiles and columns contents

R. M. Zbinden et al.

Table 2. Difference by month between the integrated content derived from $\overline{\text{MPTP}}(O_3, z, m')$ and $\overline{\text{WPTP}}(O_3, z, m')$ with $z = [2, 8\,\text{km}]$, in time coincidence, for USeast, Germany and Japan clusters with the correlation coefficient r (column 2). The differences $\overline{\text{MPTP}}(O_3, z, m') - \overline{\text{WPTP}}(O_3, z, m')$ are given in columns 4–15. The last two columns are the average and standard deviation. In each cell, the difference is expressed in % and in DU on the first and second line, respectively.

Cluster	r	unit	Jan	Feb	Mar	Apr	May	Jun	Jul	Aug	Sep	Oct	Nov	Dec	Avg	s.d.
USeast	0.949	%	−9.87	−7.88	−1.28	−4.74	−8.19	−6.45	−9.42	−14.17	−8.26	−11.02	−2.81	−8.96	−7.75	3.54
		DU	−1.79	−1.44	−0.25	−1.06	−1.94	−1.46	−2.20	−3.13	−1.62	−2.02	−0.47	−1.48	−1.57	0.77
Germany	0.984	%	−1.51	−0.89	0.85	−0.17	−1.40	−1.43	−2.71	−2.09	−4.87	−2.98	−3.03	−2.66	−1.91	1.50
		DU	−0.24	−0.15	0.16	−0.04	−0.30	−0.31	−0.59	−0.44	−0.91	−0.49	−0.48	−0.41	−0.35	0.28
Japan	0.914	%	8.34	9.69	6.33	1.50	−2.70	−4.82	−10.18	−4.51	−1.35	1.51	3.99	3.98	0.98	5.91
		DU	1.31	1.67	1.22	0.32	−0.61	−1.20	−2.10	−0.80	−0.24	0.26	0.64	0.64	0.09	1.12

ACPD
13, 14695–14747, 2013

Table 3. Pure tropospheric columns PTC(X,s) and related partial columns, UTC(X,s), MTC(X,s) and BLC(X,s), where X is O_3 and CO at season s over USeast, Germany and Japan in DU and in $\times 10^{18}$ mol cm^{-2}, respectively. These results are in bold characters. For O_3, the additional small characters in parentheses refer to previous values on incomplete tropospheric columns (TOC) and partial columns as given in Zbinden et al. (2006). MTC and UTC (bold) are derived using the new L_d definition.

		USeast				Germany				Japan			
		Spring	Summer	Autumn	Winter	Spring	Summer	Autumn	Winter	Spring	Summer	Autumn	Winter
O_3	(TOC)	(33.4)	(37.8)	(26.8)	(24.0)	(32.0)	(34.0)	(25.1)	(23.9)	(36.1)	(31.5)	(27.5)	(26.4)
	PTC	**34.82**	**39.24**	**27.68**	**25.05**	**33.05**	**35.31**	**26.55**	**24.97**	**37.60**	**34.52**	**29.66**	**27.44**
	(UTC)	(5.7)	(8.1)	(4.8)	(3.8)	(5.3)	(6.2)	(4.2)	(4.0)	(5.9)	(7.2)	(5.0)	(3.5)
	UTC	**9.14**	**7.67**	**7.34**	**6.93**	**7.76**	**7.64**	**6.05**	**6.31**	**9.54**	**6.37**	**6.34**	**7.68**
	(MTC)	(20.0)	(20.3)	(16.2)	(15.6)	(19.6)	(20.3)	(16.0)	(15.3)	(21.3)	(17.8)	(16.1)	(16.4)
	MTC	**17.21**	**22.40**	**14.08**	**12.41**	**17.63**	**19.86**	**15.13**	**13.37**	**18.56**	**21.43**	**16.61**	**12.69**
	(BLC)	(8.3)	(9.4)	(6.2)	(5.4)	(7.5)	(7.7)	(5.1)	(5.0)	(9.5)	(6.4)	(6.6)	(7.1)
	BLC	**8.47**	**9.17**	**6.27**	**5.70**	**7.66**	**7.81**	**5.37**	**5.30**	**9.50**	**6.72**	**6.70**	**7.08**
CO	**PTC**	**2.55**	**2.17**	**2.06**	**2.35**	**2.50**	**1.96**	**2.04**	**2.47**	**3.05**	**2.50**	**2.39**	**2.61**
	UTC	**0.47**	**0.28**	**0.39**	**0.39**	**0.38**	**0.28**	**0.29**	**0.39**	**0.53**	**0.32**	**0.32**	**0.43**
	MTC	**1.12**	**1.10**	**0.86**	**0.99**	**1.15**	**0.96**	**0.94**	**1.07**	**1.31**	**1.28**	**1.15**	**1.07**
	BLC	**0.96**	**0.80**	**0.81**	**0.97**	**0.97**	**0.72**	**0.81**	**1.02**	**1.21**	**0.90**	**0.93**	**1.11**

ACPD

13, 14695–14747, 2013

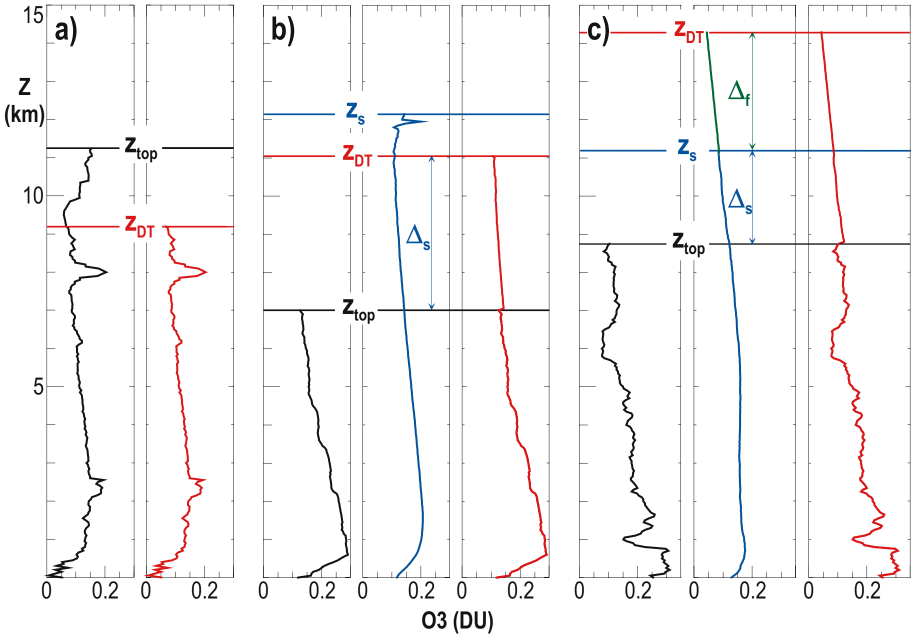

Fig. 1. Pure tropospheric profiles up to z_{DT}, $PTP(O_3, z, t)$ (red), from three typical individual MOZAIC profiles, $MP(O_3, z, t)$ (black), using the preliminary seasonal tropospheric profile, $\overline{TP}(O_3, z, s)$ (blue). For **(a)** $z_{DT} < z_{top}$; **(b)** $z_{top} < z_{DT} < z_s$; and **(c)** $z_{DT} > z_s$. Δ_s and Δ_f will be the layer filled using $\overline{TP}(O_3, z, s)$ (blue) and $Mfit_s$ (green), respectively. See the text for more explanations on z_{DT}, z_s and z_{top}.

ACPD
13, 14695–14747, 2013

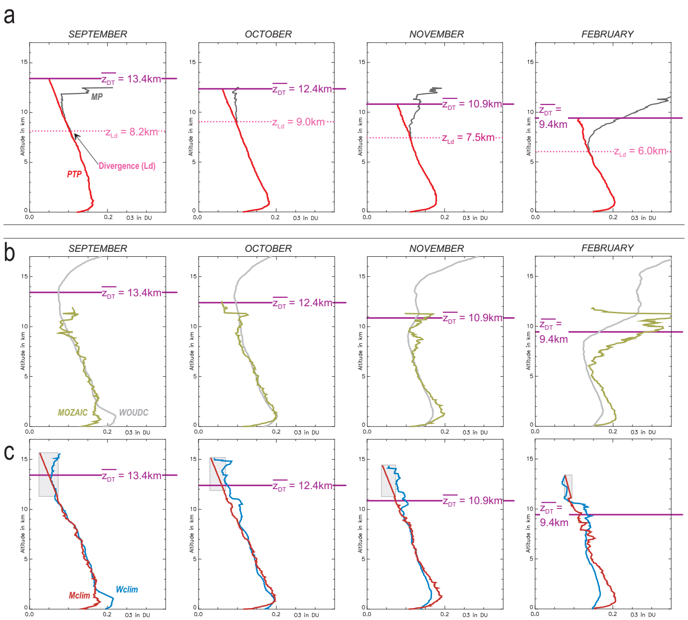

Fig. 2. Methodology **(a)** and validation **(b, c)** illustrated with data sets of MOZAIC over Japan and WOUDC sondes at Tateno (1994–2006) focusing on September, October, November and February profiles (left to right) with various $\overline{z_{\mathrm{DT}}}$ (purple horizontal line), on a monthly-averaged basis. In **(a)**, using the full MOZAIC data set $\overline{\mathrm{MP}}(\mathrm{O_3},z,m)$ with $z=[z_0,z_{\mathrm{top}}]$ (black) and $\overline{\mathrm{PTP}}(\mathrm{O_3},z,m)$ with $z=[z_0,z_{\mathrm{DT}}]$ (red). The altitude where $\overline{\mathrm{MP}}(\mathrm{O_3},z,m)$ diverges from $\overline{\mathrm{PTP}}(\mathrm{O_3},z,m)$ is defined as z_{Ld}, the dotted pink line. In **(b)**, using time-coincident data sets $\overline{\mathrm{MP}}(\mathrm{O_3},z,m')$ (green – MOZAIC) and $\overline{\mathrm{WP}}(\mathrm{O_3},z,m')$ (grey – WOUDC). In **(c)** using only tropospheric data sets between z_0 and z_{DT} of the time-coincident data sets $\overline{\mathrm{MPTP}}(\mathrm{O_3},z,m')$ (red – MOZAIC) and $\overline{\mathrm{WPTP}}(\mathrm{O_3},z,m')$ (blue – WOUDC). The impact of the $\mathrm{Mfit_s}$ filling is underlined on the figure with a grey shaded rectangle. Horizontal axis is O_3 expressed in DU and vertical axis is altitude in km.

ACPD
13, 14695–14747, 2013

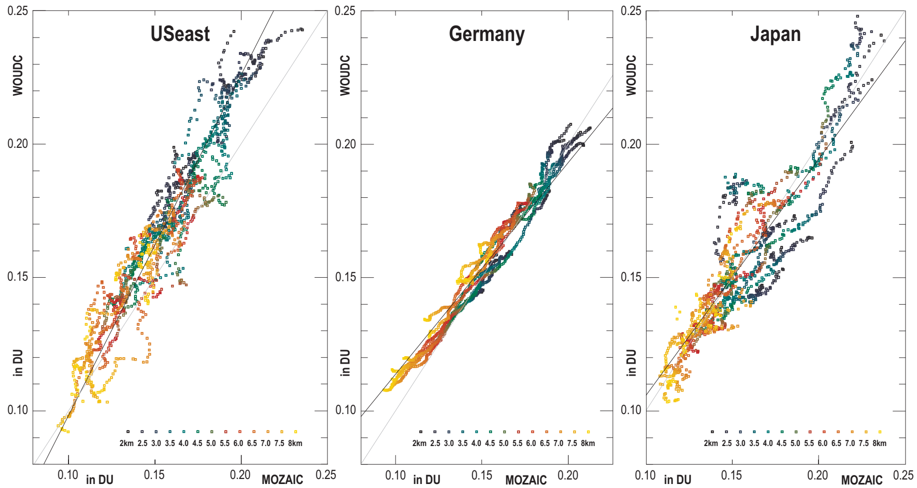

Fig. 3. Comparison of MOZAIC $\overline{\text{MPTP}}(O_3, z, m')$ and WOUDC $\overline{\text{WPTP}}(O_3, z, m')$, with z between 2 and 8 km in time coincidence, over USeast (left), Germany (middle) and Japan (right). Measurement altitudes refer to colour scale, from black (2 km) to yellow (8 km). The black line is the overall fit for each site and the grey line, the bisector. All values are in DU.

ACPD
13, 14695–14747, 2013

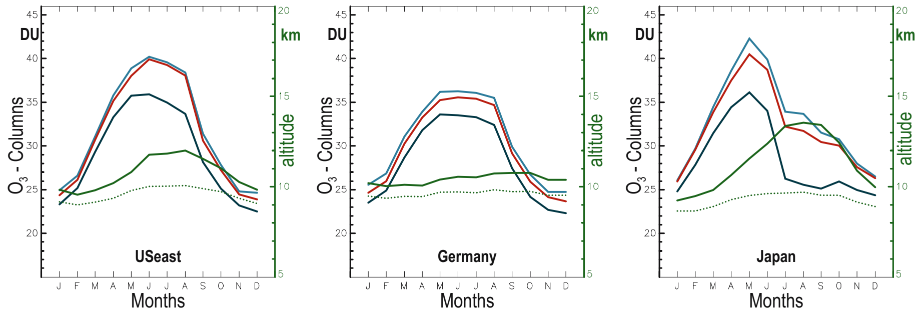

Fig. 4. Validation and impact of Δ on the pure tropospheric columns based on USeast, Germany and Japan seasonal cycles by comparing: $\overline{\mathrm{TC}}(\mathrm{O_3}, m)$, exactly what MOZAIC has measured in the troposphere (dark blue line); $\overline{\mathrm{PTC}}(\mathrm{O_3}, m)$, the MOZAIC pure tropospheric ozone column (red line); $\overline{\mathrm{MWPTC}}(\mathrm{O_3}, m)$, the composite MOZAIC-WOUDC tropospheric ozone column (blue line). All columns are expressed in DU. Δ is the layer between z_{top} (dotted green line) and z_{DT} (solid green line), in km (right green vertical axis).

ACPD
13, 14695–14747, 2013

Pure Tropospheric O_3 and CO profiles and columns contents

R. M. Zbinden et al.

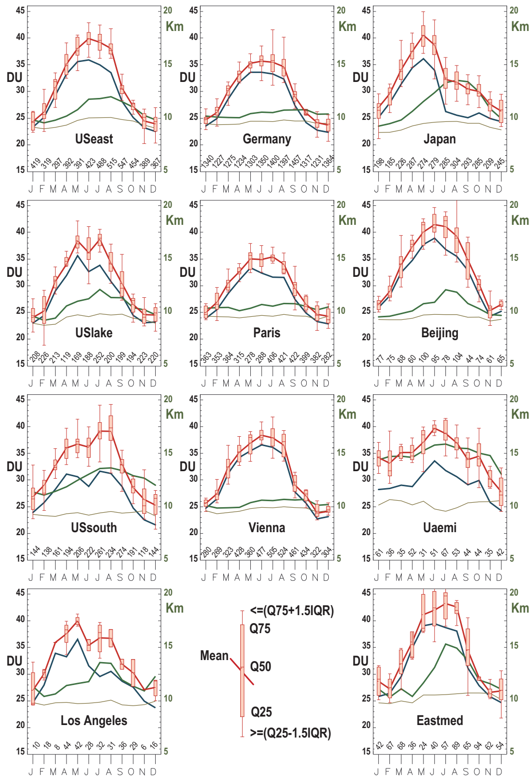

Fig. 5. Cycles of $TC_m(O_3)$, in blue, and $PTC_m(O_3)$ box and whisker, in red, expressed in DU by referring to left vertical axis for USeast, USlake, USsouth, Los Angeles, Germany, Paris, Vienna, Japan, Beijing, Uaemi and Eastmed. z_{DT} is the thick green line and z_{top} the thin green line, both referring to the right vertical axis in km. Monthly sampling frequency of each site is provided above the x-axis. Box uses the quartiles [Q25, Q50, Q75]. The end of box whiskers are the ≥Q25-1.5IQR or ≤Q75+1.5IQR.

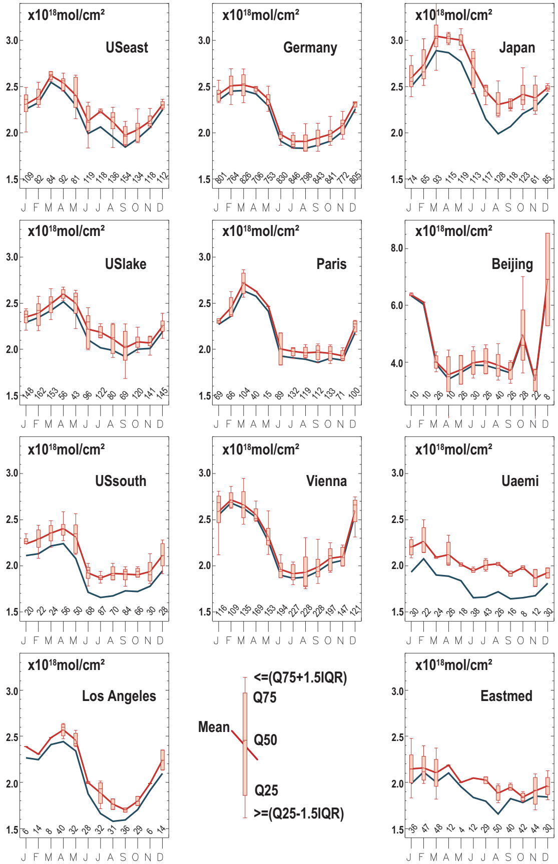

Fig. 6. Same as Fig. 5 but for CO, expressed in $\times 10^{18}$ mol cm^{-2}. Note that only Beijing is plotted with a specific scale.

ACPD
13, 14695–14747, 2013

Pure Tropospheric O_3 and CO profiles and columns contents

R. M. Zbinden et al.

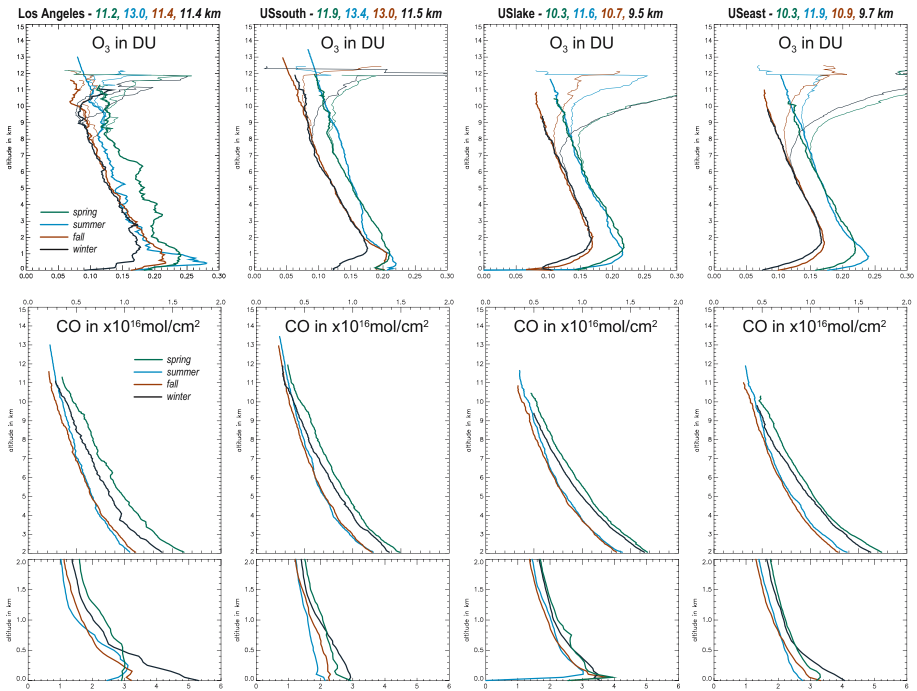

Fig. 7. Seasonal profiles for O_3 and CO (top and bottom) over Los Angeles, USsouth, USlake and USeast (left to right). For O_3, $MP_s(O_3)$ are the thin lines and $PTP_s(O_3)$ are the thick lines limited to the seasonal z_{DT} and expressed in DU. The CO includes only the $PTP_s(CO)$, expressed in $\times 10^{16}$ mol cm^{-2}, using different horizontal scales and two vertical scales for altitude (0–2 km bottom, 2–15 km top). The spring, summer, autumn and winter profiles are in green, blue, brown and black, respectively. The seasonal z_{DT} are given using the seasonal colours on the top of each site plot, in km.

ACPD
13, 14695–14747, 2013

Pure Tropospheric O_3 and CO profiles and columns contents

R. M. Zbinden et al.

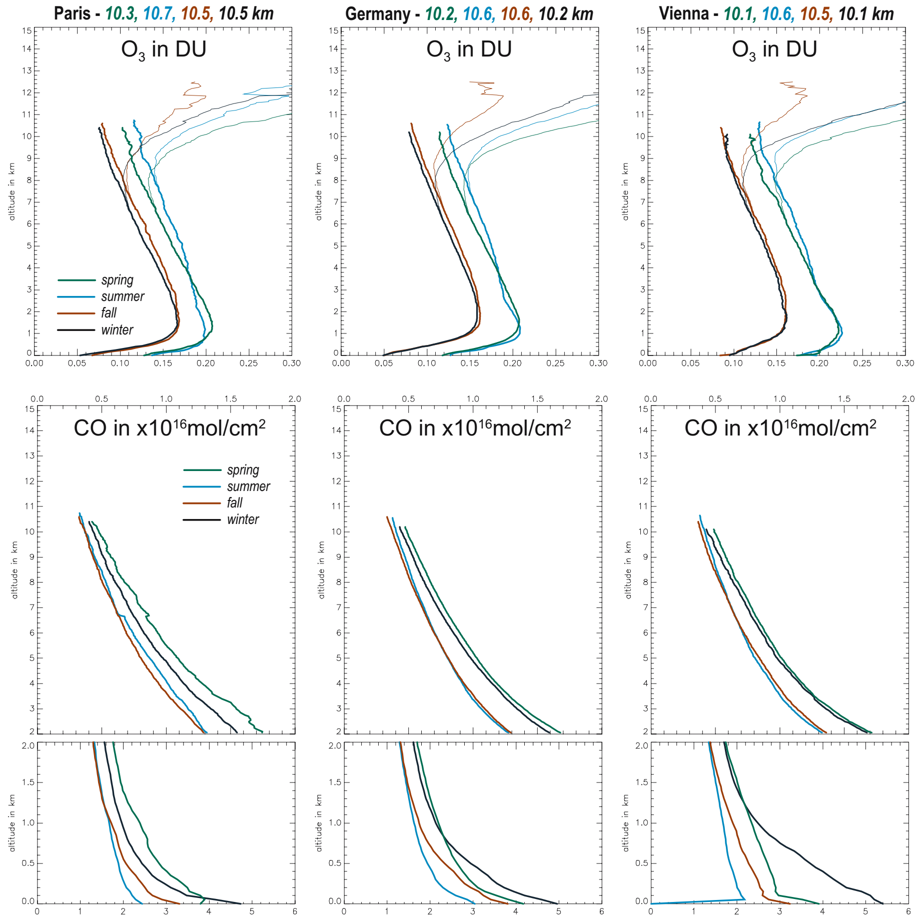

Fig. 8. Same as Fig. 7 but for Paris, Germany and Vienna.

ACPD
13, 14695–14747, 2013

Pure Tropospheric O_3 and CO profiles and columns contents

R. M. Zbinden et al.

Title Page
Abstract | Introduction
Conclusions | References
Tables | Figures
◀I | ▶I
◀ | ▶
Back | Close
Full Screen / Esc
Printer-friendly Version
Interactive Discussion

ACPD
13, 14695–14747, 2013

Title Page
Abstract
Introduction
Conclusions
References
Tables
Figures
◀|
|▶
◀
▶
Back
Close
Full Screen / Esc
Printer-friendly Version
Interactive Discussion

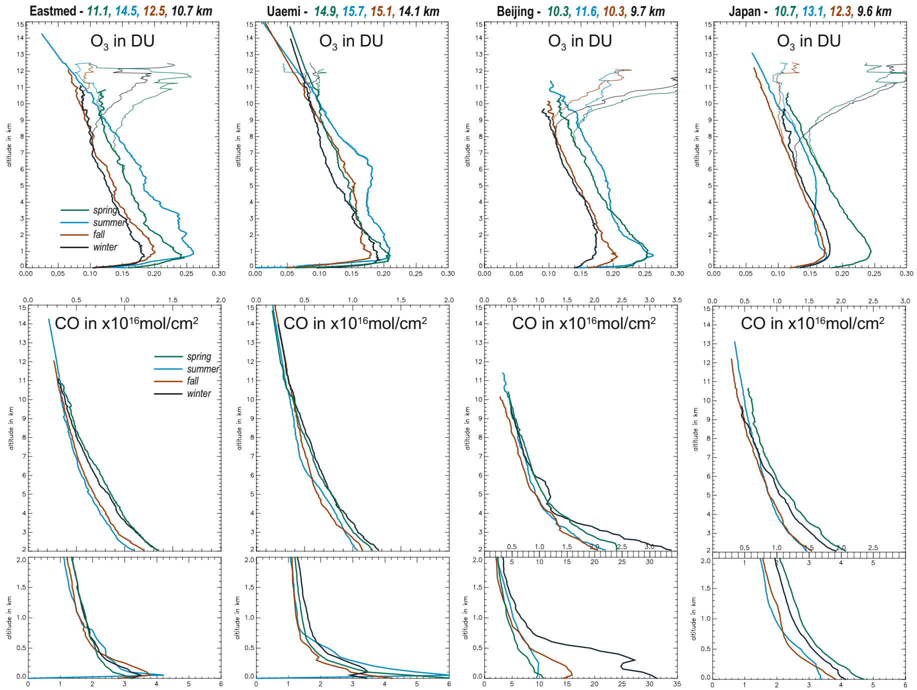

Fig. 9. Same as Fig. 7 but for Eastmed, Uaemi, Japan and Beijing, from left to right. Note the horizontal CO scale changes for the 0–2 km exclusively for Beijing and 2–15 km for Japan and Beijing.

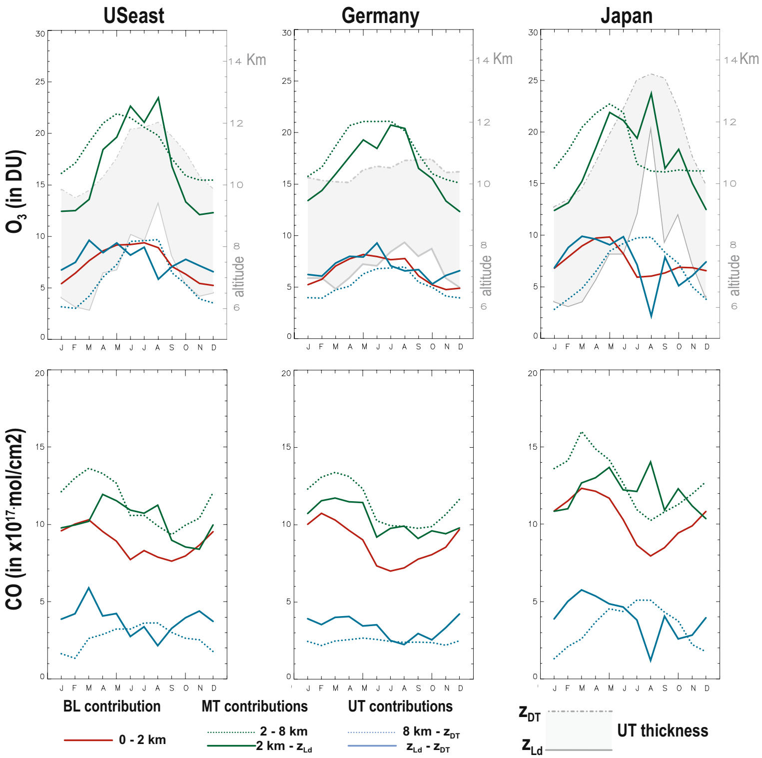

Fig. 10. Tropospheric partial columns: BLC (red), MTC (green) and UTC (blue) for USeast, Germany and Japan (left to right). The previous MTC [2–8 km] and UTC [8 km–z_{DT}] are the coloured dotted lines and, by using monthly-varying limits, the new MTC results [2 km–z_{Ld}], and the UTC [z_{Ld}–z_{DT}] are the coloured thick lines. O_3 (top row) and CO (bottom row) are expressed in DU and in mol cm^{-2}, respectively. Shaded area on O_3 plots highlights the UTC thickness (between z_{DT} and z_{Ld}, the dotted dashed line and the grey line respectively), referring to the right vertical scale in km.

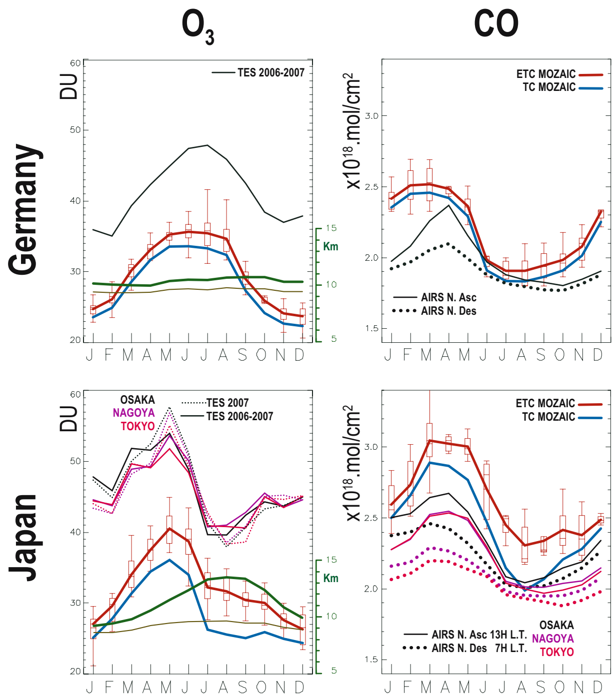

Fig. 11. Seasonal cycles MOZAIC PTC and satellite comparison, i.e. $PTC_m(O_3)$ with TES O_3 tropospheric columns (left, in DU) and $PTC_m(CO)$ with AIRS CO total columns (right, in $\times 10^{18}$ mol cm^{-2}) over Germany (top) and Japan (bottom). MOZAIC TC is the blue line and PTC the red line with box and whiskers (as on Fig. 5). z_{DT} is the thick green line and z_{top} the thin green line, both referring to the right vertical axis of the O_3 plots in km (as on Fig. 5). The satellite results are plotted over Germany in black, and over Japan in pink, black and purple for Tokyo, Osaka and Nagoya, respectively. AIRS CO results are given twice a day for ascending node (13:00 LT, solid line) and descending node (07:00 LT, dotted line). O_3 tropospheric columns from TES in 10^{18} mol cm^{-2} over the periods 2006–2007 or 2007 (solid lines or dotted lines) are converted into DU dividing by 2.686×10^{16}.

ACPD
13, 14695–14747, 2013